Evaluation of Ion Transfer Capillary Geometry on Sensitivity of a Desorption Electrospray Ionization and Mass Spectrometry System

by

Nagashumrith Venkata Vinakollu

Bachelor of Science in Mechanical Engineering.
Georgia Institute of Technology, 2018

Submitted to the Department of Mechanical Engineering
in Partial Fulfillment of the Requirements for the Degree of

Master of Engineering in Advanced Manufacturing and Design

at the

MASSACHUSETTS INSTITUTE OF TECHNOLOGY

February 2021

Author . . . . . .
Department of Mechanical Engineering
September 10, 2020

Certified by . . . . . .
David E. Hardt
Ralph E. and Eloise F. Cross Professor in Manufacturing, Mechanical Engineering
Thesis Supervisor

Accepted by. . . . . .
Nicolas Hadjiconstantinou
Chairman, Department Committee on Graduate Theses

This page is intentionally left blank

Evaluation of Ion Transfer Capillary Geometry on Sensitivity of a Desorption Electrospray Ionization and Mass Spectrometry System

by

Nagashumrith Venkata Vinakollu

Bachelor of Science in Mechanical Engineering,

Georgia Institute of Technology, 2018

Submitted to the Department of Mechanical Engineering

on September 10, 2020 in Partial Fulfillment of the Requirements for the Degree of

Master of Engineering in Advanced Manufacturing and Design

Abstract

This research examines the effect of ion transfer capillary geometry on the sensitivity of the Desorption Electrospray Ionization – Mass Spectrometry (DESI-MS) process. Previous work has shown that heating the ion transfer capillary to 450˚C will improve the resolution of images taken by the DESI-MS owing to increased ion desolvation. This thesis studies how changing the inner diameter and cross-sectional profile of the capillary can improve ion desolvation by increased heat transfer to the center of the flow. Increasing heat transfer efficiency can obviate such high temperatures and will increase flexibility in the design of the capillary heater.

The setup of this experiment involved making modifications to existing components to allow for rapid testing of many ion transfer capillary geometries. Mass spectrum data for sample sections of pig liver were collected, as these biological samples are acceptably homogenous with a known mass-to-charge (*m/z*) ratio of 885. Signal intensity within the 880- 890 *m/z* range is analyzed to reveal the impact of capillary geometry. Sources of variation, such as within-sample variation and sample-to-sample variation, are characterized to reveal the true impact of the variables.

The results show that decreasing max particle distance from a wall can increase the sensitivity of the ion flow to heating. The best capillary cross-section provides nearly a 4x increase in sensitivity when compared to a circular capillary with a similar flow area. Pursuing these capillary designs will improve not only sample resolution and imaging time but also the client satisfaction of the Waters DESI- MS system.

Thesis Supervisor: David Hardt

Title: Ralph E. and Eloise F. Cross Professor in Mechanical Engineering

This page is intentionally left blank

Acknowledgments

This thesis would not have come together without the support of many wonderful people.

I would like to thank the team at Waters for giving me the opportunity to work on this project. First, thank you, Joe Michienzi, for mentoring me during the DESI project and giving Daniel and me the freedom to pursue our own ideas, no matter how wild they seemed. Thank you to Mike Fogwill, Jeffrey Mussachio, Mike Leal, Wade Leveille, Ashwin Meyyapan, Patrick Brophy, Greg Roman, and Sonya-Wilson Thomas for all your support and this project such a positive experience.

To the Waters-MIT team, Daniel, Robyn, and Yang, thanks for being such great pals throughout the year. I truly enjoyed working with all of you and know you guys will do great in your future endeavors.

I would also like to thank Prof. Dave Hardt and Jose Pacheco for giving me the opportunity to be apart of the 2020 MEng cohort, as well as your support throughout the year. I have learned so much this past year because of the great program that you both put together.

Thank you to the rest of the MEng cohort for making this a memorable year. It has been a bit of a rollercoaster year, and I wouldn't have made it off without you guys.

Finally, I would like to thank my parents and little sister for their never-ending support throughout my life. Without your support, I really would not have been able to get this far. Knowing that you are there for me gives me the strength to push through whatever life throws at me.

This page is intentionally left blank

Table of Contents

This page is intentionally left blank

LIST OF FIGURES

LIST OF TABLES

LIST OF EQUATIONS

ABBREVIATIONS

ESI	Electrospray Ionization
DESI	Desorption Electrospray Ionization
MALDI	Matrix-Assisted Laser Desorption/Ionization
MS	Mass Spectrometry
ANSYS	Analysis Systems
LC	Liquid Chromatography
UPLC	UltraPerformance Liquid Chromatography
HPLC	High-Performance Liquid Chromatography
TOF	Time- of- Flight
HDMS	High Definition Mass Spectrometry
OD	Outer Diameter
ID	Inner Diameter
SST	Stainless Steel
EDM	Electrical Discharge Machining
CAD	Computer-Aided Design
CTE	Coefficient of Thermal Expansion
SLA	Stereolithography
IPA	Isopropanol Alcohol
PSU	Power Supply Unit
SLPM	Standard Liters Per Minute

CHAPTER 1

INTRODUCTION

1.1 Problem Statement

This project aims to improve the Desorption Electrospray Ionization (DESI) system used in conjunction with a mass spectrometer to collect higher resolution images of samples. Specifically, the ion transfer capillary used to transfer ionized molecules from the sample to the mass spectrometer is studied to improve ion transfer efficiency. The design and heat transfer characteristics of the ion transfer capillary are experimentally evaluated to test signal intensity.

This primary focus of the thesis is to experimentally evaluate characteristics of the ion transfer capillary that contribute to the DESI-MS system resolution.

1.2 Motivation

Waters utilizes the DESI system in its line of mass spectrometry imaging services. These services offer high-resolution imaging of biological and pharmaceutical samples. Advancing the DESI technology at Waters will improve the quality of these services.

The ion transfer capillary is one of the most critical parts of the DESI-MS system, as it facilitates the transfer of ionized molecules from the sample to the MS. Research contributing to the design of the ion transfer capillary will provide higher resolution imaging, increasing the value of Waters' mass spectrometry services.

1.3 Objective

Previous work at Waters has shown that heating the ion transfer capillary will increase the resolution of the image. The primary objective of this project will be to improve the heating efficiency of the ion transfer capillary. Doing so will allow for greater flexibility in the design of the heating device, as an increased heating efficiency will allow lower capillary temperatures to provide the same benefit. The secondary objective will be to advance the design of the heater to improve user satisfaction.

1.4 Project Scope

The scope of the project is to study the impact of two key parameters of the ion transfer capillary on ion transfer efficiency and heat transfer efficiency. Specifically, the inner diameter and the cross-sectional profile are modified to study their impact on the max signal intensity of the mass spectrum. The results from the experiment are used to develop recommendations for ion transfer capillary geometry and heater design.

1.5 Thesis Structure

This thesis compromises nine chapters. Chapter one outlines the goals of the project, and chapter two presents the Waters Corporation company background. Chapter three details the DESI-MS system and presents prior work regarding the ion transfer capillary. Chapters four through six describe the experiment, as well as explain the setup and procedure. Chapter seven overviews data acquisition and analysis techniques. In chapter eight, the results of the experiments are presented. Finally, chapter nine reviews the key takeaways of the experiments and provides recommendations on future work to Waters regarding the design of the ion transfer capillary and heater.

1.6 Statement of Collaboration

This project is done in close collaboration with Chun- Cheng Hsu, a colleague in the Master of Advanced Manufacturing and Design program. The experiment was designed and executed through constant discussions with Hsu. This thesis focuses on the setup and data processing for the first round of results with .0787" brass capillaries. Hsu's thesis will focus on the simulation of heat transfer and flow characteristics of various capillaries [1]. As Hsu will continue the project after the completion of this thesis, his thesis will also include the results of forthcoming capillary geometries.

CHAPTER 2

BACKGROUND

2.1 Waters Corporation

Waters Corporation was founded in 1958 by Jim Waters as a research firm [2]. Over the years, the firm grew from a basement office in Framingham, Massachusetts, to an organization with facilities in 35 countries [3]. Their headquarters located in Milford, Massachusetts contains their primary research division, along with their Advanced Manufacturing Center. Waters expertise in chemical analytical techniques pertaining to liquid chromatography and mass spectrometry has propelled them to a $1.9 billion corporation [2]. Waters mission to "Deliver Benefit" is assumed by a workforce of over 7,000 employees [3]. The company is divided into two segments, Waters and TA. Waters focuses on LC-MS instruments and columns, whereas TA focuses on thermal analysis, rheometry, and calorimetry instruments [4].

2.2 Waters Products and Services

Waters provides laboratory services analytical equipment to over 40,000 customers around the world. Fifteen manufacturing facilities produce critical analytical and laboratory equipment [3]. These services span a broad spectrum, from quality and reliability control to data analysis [5]. Their products include LC-MS instruments, laboratory informatics, and chromatography consumables.

2.2.1 Waters Services

Waters offers services designed to improve its clients' workflow and satisfaction. Their customer success portal provides a wealth of knowledge regarding Waters products. Their online

portal allows clients to request spare parts and select the right chemistries for consumables. Waters ensures the lasting quality of their products with their instrument services. Along with their software, these services allow clients to validate their system to maintain compliance. In 2019, these services compromised of 35% of revenue for the company [4]. Their primary competitors include Agilent Technologies, Thermo Fisher Scientific, and PerkinElmer [4]. Waters ensures that clients can unlock the full potential of their products through these services.

2.2.2 Liquid Chromatography Instrument

Waters' liquid chromatography instruments consist of their HPLC and UPLC lines. The purpose of these instruments is to breakdown a sample and measure the number of unique chemical components that exist within. UPLC differs from HPLC in that it uses smaller particles in its packed columns. Combined with a novel instrument, this allows for testing a more comprehensive range of analytes, with improved processing speeds [4]. The Milford, Massachusetts facility is the primary producer of their LC product line.

They primarily serve life science and pharmaceutical industries, as these can be used to develop new drugs and ensure their quality. Additional applications in the consumer product, chemical, and environmental industries also exist. Waters offers flexibility in the deployment of their instruments from client to client. They tailor their HPLC and UPLC instruments to the needs of their consumer and offer different levels of process automation.

2.2.3 Consumables

The LC instruments require consumable products that must be replenished over time. The primary consumables are chromatography columns. Chromatography columns are essentially steel tubes packed with material that is used as a separation medium. The interactions which take place

within the columns allow for classification of various chemical components within a sample. Waters manufactures all parts of the column, from the polymer-based packing material to the column itself. The vertical integration of column manufacturing allows Waters to maintain a high level of quality and respond quickly to customer needs [4].

2.2.4 Mass Spectrometry Instruments

In addition to LC instruments, Waters also produces MS and LC-MS instruments. MS technology allows for chemical identification and quantification through analysis of molecular mass. Waters has recently begun integrating their LC and MS systems, as clients tend to use them together. Facilities in Wilmslow, England and Wexford, Ireland produce their MS product line [4]. They manufacture a range of MS instruments and software platforms to fit client needs. This project specifically uses the SYNAPT™ G2-S MS, a quadrupole TOF instrument, along with their MassLynx™. Software. Waters' constant innovation and production of quality LC-MS instruments has elevated them to one of the global leaders in this industry [4].

2.3 Waters- MIT Collaboration

Waters and MIT have been collaborating since 2013. Each year, Masters students in the Advanced Manufacturing and Design program at MIT have taken on projects to improve the manufacturing capability and operational efficiency of Waters. For example, students in 2018 focused on optimizing inventory location in the Global Distribution Center located in Franklin, Massachusetts [6], [7]. In 2019, students developed an automated vial inspection system [8], [9].

This year, four students from MIT are working with Waters. Robyn Lee and Yang Wang, are analyzing material flow at the Milford, Massachusetts facility. Lee’s project focuses on backups occurring on the conveyor belt transporting finished goods from assembly to kitting [10].

Wang's project focuses on the shortcomings of the current e-Kanban system implemented by Waters [11]. This project, in collaboration with Daniel Hsu, focuses on improving the sensitivity of a Waters MS system through modifications to the ion transfer capillary.

CHAPTER 3

MASS SPECTROMETRY OVERVIEW

3.1 Mass Spectrometry

Mass spectrometry is an analysis technique developed to measure the mass of a charged molecule. Scientists use MS technology for a variety of purposes, from discovering new drugs to analyzing water quality. The technology has been around for quite a while; the first mass spectrometers were developed 100 years ago [12]. Over the years, new MS instrument designs have increased detection capabilities, allowing scientists to study more types of samples.

One of the most common forms of MS technology involves the magnetic deflection of charged particles (Figure 1). The four key steps in the process are ionization, acceleration, deflection, and detection [13]. During ionization, molecules acquire a charge, either positive or negative depending on the ionization technique. These charged molecules, now ions, are then accelerated by an ion lens that directs them towards the mass analyzer. Next, an electromagnet provides a magnetic field which deflects ions. Heavier ions are deflected less than lighter ions. Finally, a detection device analyzes the magnitude of deflection to find the ion's mass/charge (m/z) ratio.

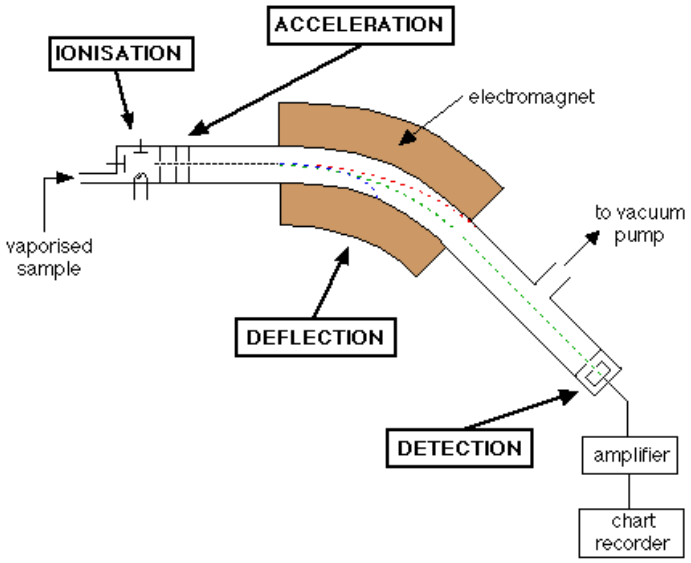

Figure 1: High- Level Diagram of Mass Spectrometer [13]

The underlying principle can be derived from Newton's second law of motion and the Lorentz force law, which results in Equation 1. Since the velocity of the ions is modulated by the acceleration device and the electromagnet is supplying a constant and known magnetic flux, the radius of deflection can be used to acquire an ion's m/z ratio.

Equation 1: Mass/Charge Ratio of Deflected Ions

$$\frac{m}{q} = \frac{rB}{V}$$

$$\frac{m}{q} = mass/charge\ ratio$$

$$r = deflection\ radius$$

$$B = Magentic\ Flux\ Density$$

$$V = velocity$$

The output of MS is known as a mass spectrum (Figure 2). A mass spectrum displays the *m/z* on the x- axis and the intensity on the y- axis. A mass spectrum displays a count of ions at different *m/z.* The mass spectrum reveals valuable information regarding the chemical composition of a sample. Compounds with known molecular masses can be identified in a sample's mass spectrum.

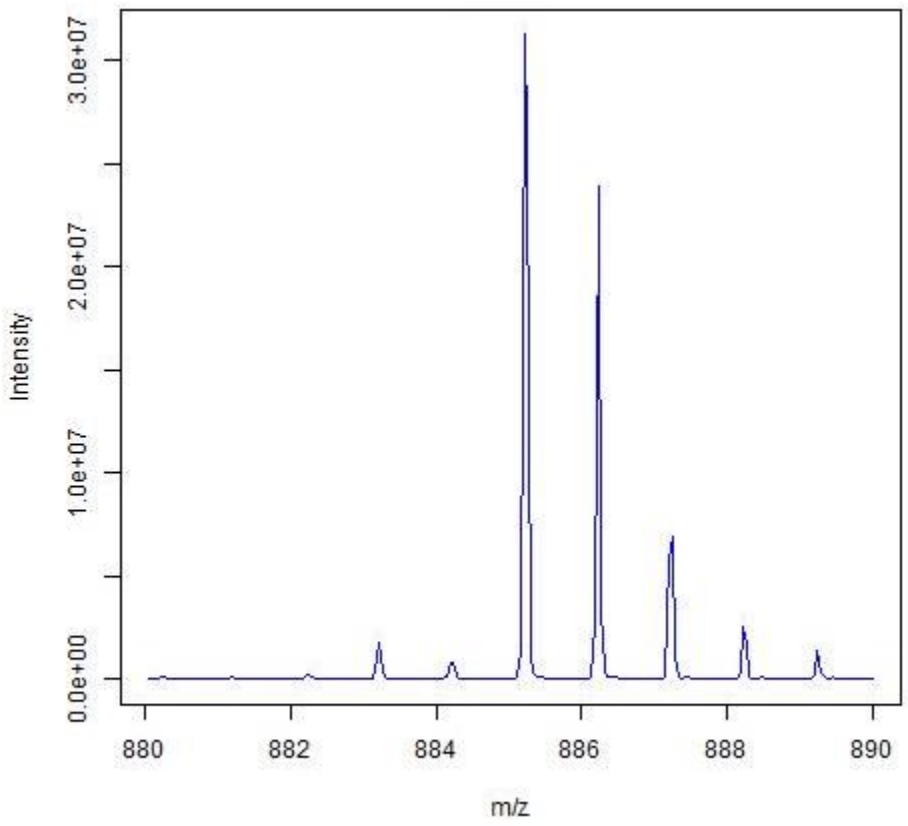

Figure 2: Mass Spectrum of a Pig liver Section

3.2 Desorption Electrospray Ionization

MS systems employ several different ionization methods. Among the most commonly used are matrix-assisted laser desorption/ionization (MALDI), electrospray ionization (ESI), and desorption electrospray ionization (DESI).

MALDI is used primarily for the ionization of solid samples. It involves targeting a matrix-infused sample with a laser and exciting molecules into the gas phase [14]. The composition of the matrix is selected based on the type of sample. UV lasers are the most popular, while IR lasers are also used. MALDI can be performed in a vacuum and at atmospheric pressure, making it a versatile ionization technique.

In ESI, a solution containing the analyte is sprayed through a needle charged to a few kilovolts. The charged droplets containing the analyte molecules are captured by a glass capillary and transported to a chamber. In this chamber, the droplets are heated to desolve the ions from the surrounding solvent (Figure 3). Once desolved, the ions are suitable for mass analysis by the detector [15].

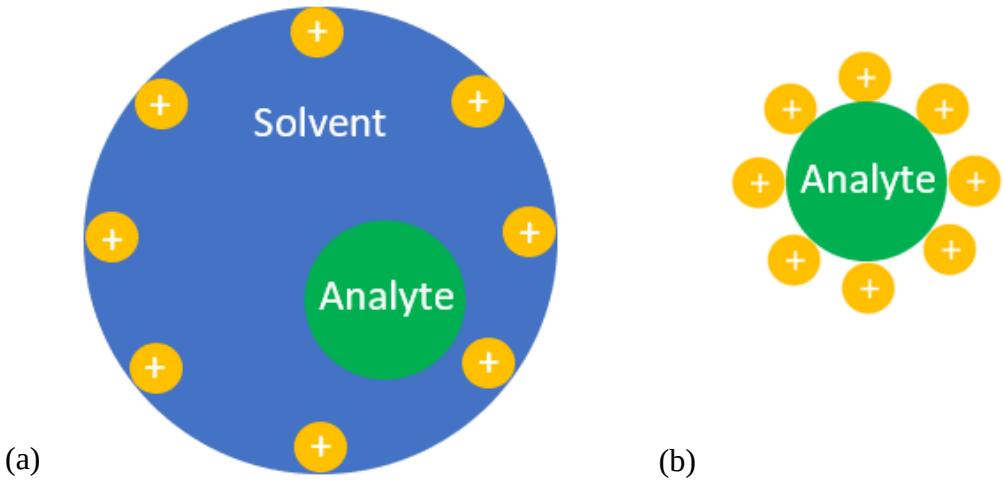

Figure 3: (a) Sample analyte entrenched in a charged droplet. (b) Analyte is desolved, and forms an ion with a m/z.

DESI is an ionization technique similar to ESI. The key difference is that ionization can take place in ambient conditions. DESI can also ionize nonpolar compounds such as cholesterol and carotene, unlike ESI [16]. As the process can take place in ambient conditions, sample preparation is limited. For example, biological samples such as pig liver can be cut and analyzed directly. The versatility to ionize both solids and solvents in ambient conditions make DESI a prime method for rapidly analyzing samples in the field.

The first step of DESI involves a sprayer emitting a plume of charged solvent (Figure 4). The solvent is typically a methanol-based solution. The charged solvent particles collide with the

sample. During these collisions, the molecules are ionized. The ionization mechanism depends on the characteristics of the molecule, such as its molecular weight. Once ionized, charged droplets containing the analyte are dispersed into the air. An ion transfer capillary located just above the sample captures the droplets and transfers them to the MS system. The sample stage moves throughout the process, permitting the sprayer to cover the entire target area.

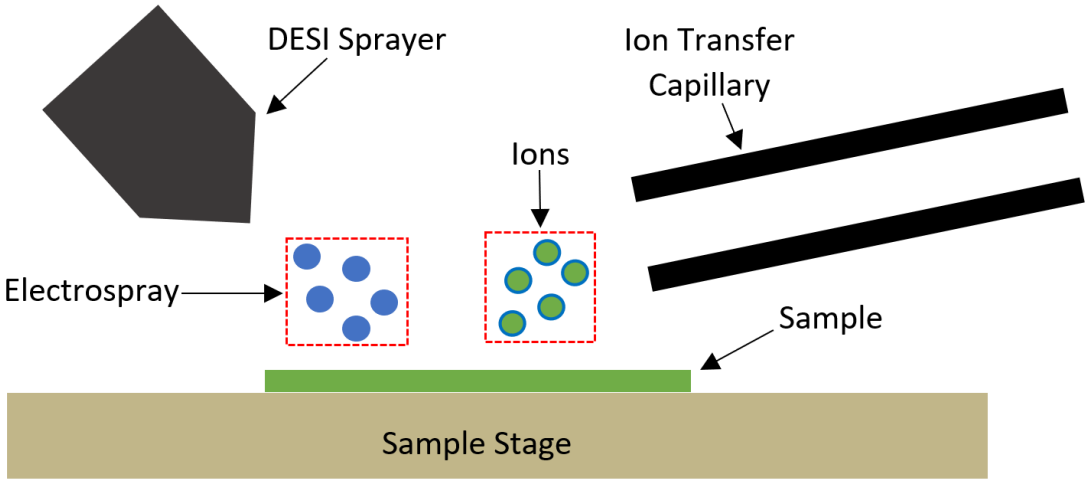

Figure 4: DESI Setup. A sprayer emits a plume of charged particles. They collide with the sample, and interact with the molecules to produce charged droplets. These droplets are captured by an ion transfer capillary and transferred to the MS.

The goal of all these ionization methods is to provide the MS the highest number of ions for analysis. The larger the ion count supplied to the MS, the higher the signal intensity on the resulting mass spectrum. The higher the signal the intensity, the higher the resolution of the sample's image from the MS. Simply put, there is an increased amount of information available at each pixel, improving the quality of the image (Figure 5).

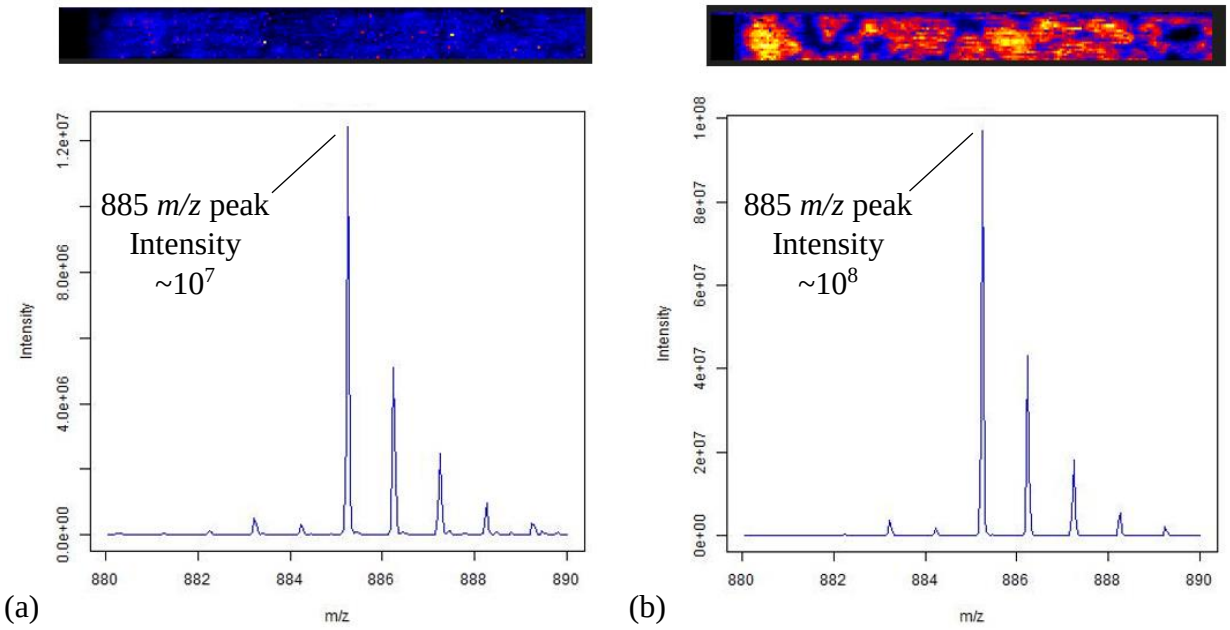

Figure 5: Section of Pig Liver imaged on an MS and its associated mass spectrum. The intensity of (b) is an order of magnitude greater than that of (a), lending itself to an image of the sample with higher clarity.

The ion count supplied to the MS depends on a variety of factors. The fluid dynamics associated with the sprayer, the position of the sprayer, and the ion transfer capillary, as well as the ion transfer capillary geometry, all affect signal intensity. As a result, DESI components can be modified to achieve higher signal intensity.

3.3 Waters MS System

Waters employs a line of MS systems. This thesis will utilize the Waters Synapt G2-Si HDMS (Figure 6). The Synapt G2- Si HDMS is a Quadrupole Time-of-Flight (Q-TOF) MS. A Q-TOF MS operates by sending desorbed ions into a quadrupole mass analyzer. A quadrupole mass analyzer consists of four electrodes subject to radiofrequency and DC voltages. They produce an electric field that sifts entering ions based on their *m/z* [17]. These ions are then pushed into a TOF

analyzer. The TOF analyzer works by accelerating ions with a voltage into a lens. The lens then reflects the ions towards a detector. The time it takes for the ions to arrive is determined by their *m/z*. The detector, which is an analog-to-digital converter, can scan a maximum of 25 ions in one sample event for their *m/z* [18]. The SYNAPT MS can sample at a rate of 30,000 spectra per second, allowing the system to generate mass spectra with high resolution [18].

Figure 6: Waters SYNAPT G2-Si HDMS [19]

The HDMS is compatible with multiple ionization techniques; in this thesis, it is paired with DESI. The setup includes a stage that has three degrees of freedom and moves the sample underneath the DESI sprayer (Figure 7). The charged droplets will enter the ion transfer capillary, travel through the nose cone and into the ion source. From the ion source, the ions will make their journey through the MS to be analyzed.

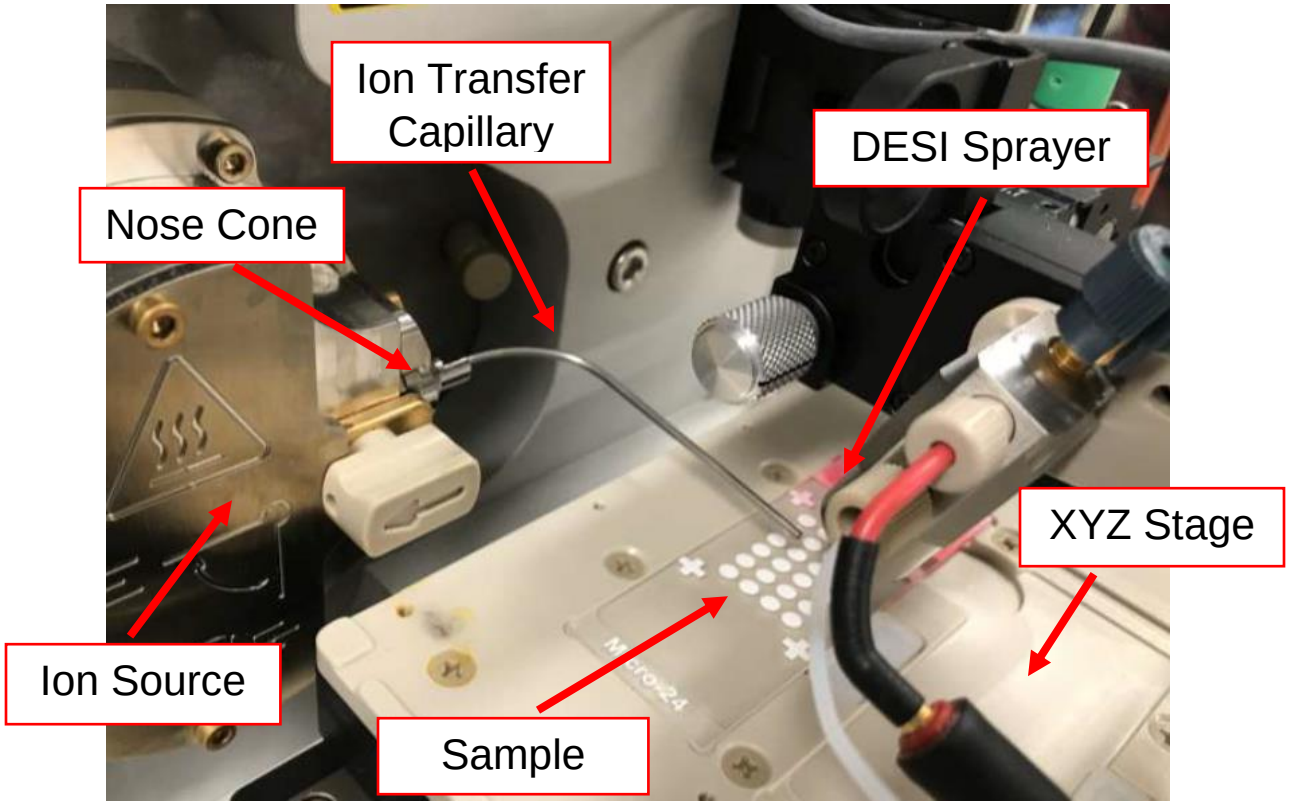

Figure 7: DESI Setup on the SYNAPT HDMS

3.4 Waters DESI-MS Projects

As previously mentioned, the components of the DESI-MS system can be modified to elicit higher signal intensity. Waters is continuing to seek these higher intensities by researching potential improvements that can be made to their system. In addition, Waters seeks to improve client satisfaction by making the system easier to use. The purpose of DESI-MS projects at Waters is centered on these two goals. The two projects proposed to MIT students focus on the DESI sprayer and DESI heater.

The DESI sprayer project focuses on the design of a new sprayer, the component which emits the charged solvent. Waters has prototyped a sprayer with a smaller emitter orifice than commercial sprayers. The smaller orifice creates a spray which remains collimated through a

longer distance than that of the original sprayer. This concept works well in practice; however, there are additional steps that must be taken before it can be commercialized. This project would address design challenges such as nozzle contamination and maintaining consistent emitter position.

The DESI heater project continues research previously conducted by Waters on the ion transfer capillary, the component which transports entrenched ions to the MS. This project focuses on improving the signal intensity of the MS by heating the ion transfer capillary and is described in greater detail in section 3.5.

3.5 Ion Transfer Capillary

The ion transfer capillary carries the entrenched ions to the MS. The design of this capillary plays a major role in defining the signal intensity of the MS system. One key factor of the ion transfer capillary is its geometry.

The geometry of the transfer capillary defines many parameters of the transport system, including flow rate and heating efficiency. For example, decreasing the capillary cross-sectional area will produce a similar decrease in flow rate [20]. A low flow rate may indicate that fewer ions are being captured to undergo MS analysis. Flow rate also influences the time an ion spends within the capillary, known as ion residence time (Equation 2). Transmitted current at the capillary is a function of ion residence time, as this time contributes to ions losses. However, lowering the cross-sectional area of the capillary can also increase ion desolvation efficiency. As the capillary is made tighter, the heating efficiency will increase. Prior work has shown that heating the flow can have an impact on signal intensity due to increased ion desolvation [21]. Understanding how changes

in geometry can affect these parameters is critical to increasing the signal intensity of the DESI-MS.

Equation 2: Ion Residence Time [22]

$$t_{res}^{0} = \frac{V * (1\ atm)}{Q_{1\ atm}}$$

$$t_{res}^{0} = Resonance\ Time\ (sec.)$$

$$V = Capillary\ Volume\ (m^3)$$

$$Q = Gas\ Flow\ Rate\ at\ 1\ atm\ (\frac{m^3}{s})$$

CHAPTER 4

EXPERIMENT OVERVIEW

In order to achieve higher signal intensity through improved ion desolvation, parameters of the ion transfer capillary that will improve heat transfer to the center of the ion flow are modified. The two parameters chosen to achieve uniform heating throughout the capillary flow area are the inner diameter and cross-sectional profile of the ion transfer capillary.

4.1 Capillary Inner Diameter

4.1.1 Inner Diameter Hypotheses

The first parameter is the inner diameter of the capillary. The current Waters capillary is made from Inconel 600 and has a .083" OD, .049" ID, and a wall thickness .017". This capillary is modified from the commercial capillary, which is made from 304SST with .062" OD and .052" ID. This wall thickness was increased to alleviate tube breaking and the material was changed to Inconel 600 to alleviate capillary oxidation at high temperatures.

The first hypothesis is that a smaller ID capillary may provide higher signal intensity due to an increased temperature boundary layer thickness (Figure 8). An increase in temperature boundary layer thickness indicates that a larger portion of the flow within the capillary is heated to temperature higher than ambient. Due to the short length of the capillaries (~5") and the high velocities (near the speed of sound at the center the flow), it is difficult to heat the center of the flow. The secondary hypothesis is that a smaller ID capillary may provide higher signal intensity due to increased flow rate [22]. The higher flow rate will contribute to a lower residence time and thus improve the transmitted current to the MS, as shown in The ion transfer capillary

carries the entrenched ions to the MS. The design of this capillary plays a major role in defining the signal intensity of the MS system. One key factor of the ion transfer capillary is its geometry.

The geometry of the transfer capillary defines many parameters of the transport system, including flow rate and heating efficiency. For example, decreasing the capillary cross-sectional area will produce a similar decrease in flow rate [20]. A low flow rate may indicate that fewer ions are being captured to undergo MS analysis. Flow rate also influences the time an ion spends within the capillary, known as ion residence time (Equation 2). Transmitted current at the capillary is a function of ion residence time, as this time contributes to ions losses. However, lowering the cross-sectional area of the capillary can also increase ion desolvation efficiency. As the capillary is made tighter, the heating efficiency will increase. Prior work has shown that heating the flow can have an impact on signal intensity due to increased ion desolvation [21]. Understanding how changes in geometry can affect these parameters is critical to increasing the signal intensity of the DESI-MS.

Equation 2.

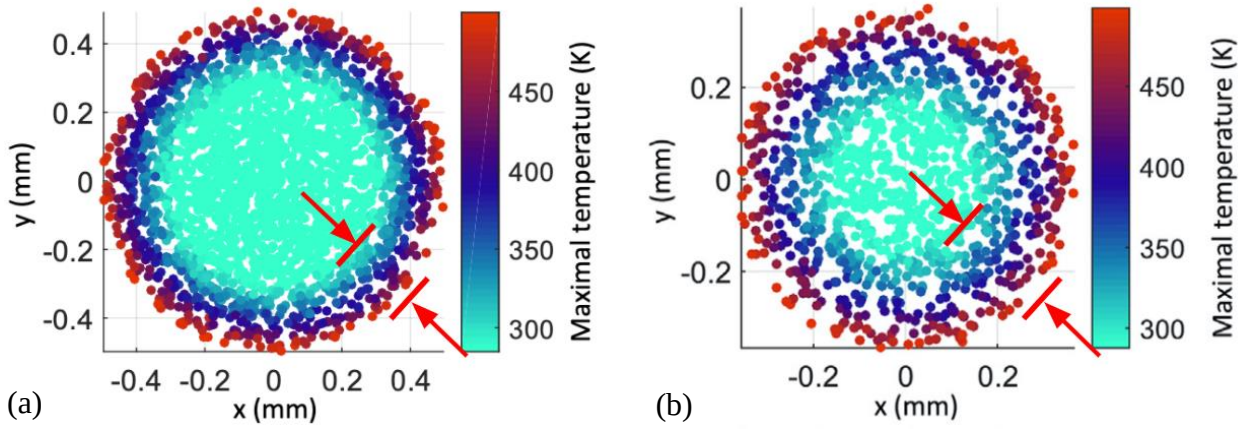

Figure 8: Simulated temperature profiles in capillaries of different ID. Capillary in (a) has a smaller ID and a larger temperature boundary layer thickness than the capillary in (b) [20]. The darker dots represent flow at a temperature closer to that of the heated wall.

4.1.2 Plan of Action

Capillaries with three different IDs are used to test these hypotheses (Table 1). These capillaries were selected for a couple of reasons. First, the OD between the capillaries is kept constant to facilitate the swapping of capillaries between experiments. Thermal simulation in ANSYS indicated that variable wall thickness does not contribute significantly to temperature differences, as seen in Figure 9 and Figure 10 [23]. Second, the vendor that supplies the hypodermic capillaries only has these in stock. This distribution of capillary IDs should provide a clear indication of differences in ion desolvation and MS signal intensity.

Table 1: Capillaries Selected for Experiment

OD (in.)	Wall Thickness (in.)	ID (in.)
0.083	0.022	0.039
0.083	0.017	0.049*
0.083	0.01	0.072

*Current Waters Capillary

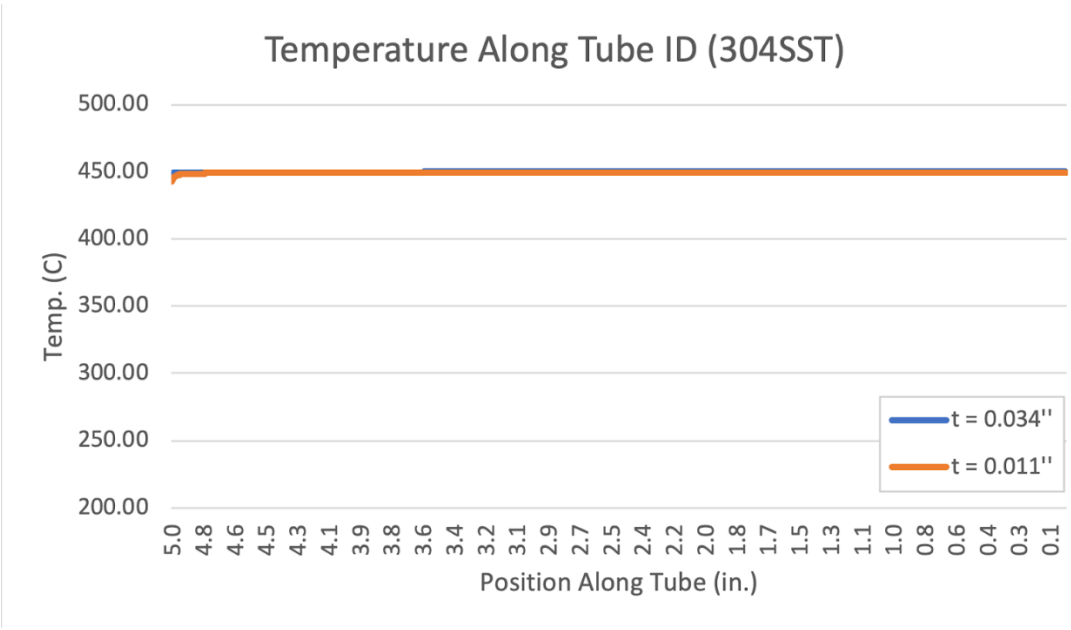

Figure 9: Temperature along capillary inner wall. The capillary wall thickness does not play a significant role in inner wall temperature.[23]

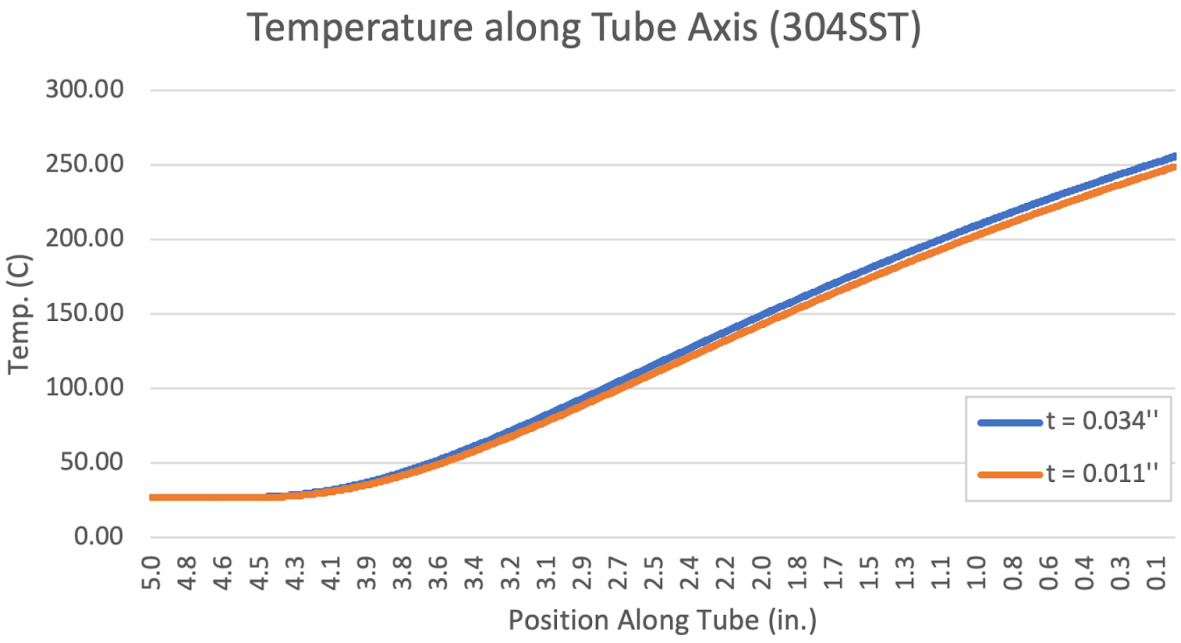

Figure 10: Temperature along capillary flow centerline. The capillary wall thickness does not play a significant role in centerline temperature.[23]

4.2 Capillary Cross-Sectional Profile

4.2.1 Cross-Section Hypotheses

The second selected parameter is the cross-sectional profile of the capillary. The hypothesis is that reduced the max particle distance to a heated wall will increase ion desolvation and increase signal intensity. In the case of profiles with smaller inner channels, the increased flow rate may also provide increased signal intensity.

Capillaries with the standard circular cross-sectional profile have a max particle distance that is simply their radius from the ID. The only way to reduce max particle distance without reducing the flow area is to change the cross-sectional profile (Figure 11). The obround shape can be used to maintain constant ion throughput while also improving ion desolvation [24]. Other cross-sections can also be explored to better understand ion desolvation within the capillary.

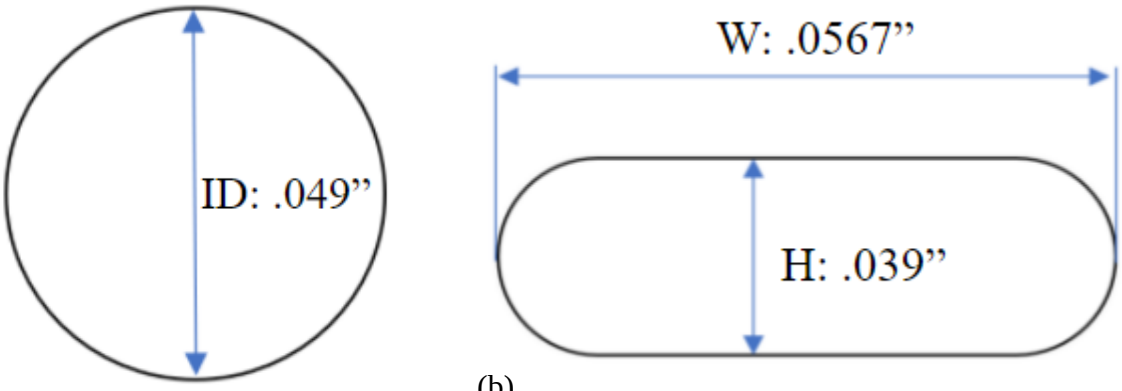

(a) Circular Cross Section
Area: 1.88E-3 in.^{2}
Max Particle Distance: .0245”

(b) Obround Cross- Section
Area: 1.88E-3 in.^{2}
Max Particle Distance: .0195”

Figure 11: Circular vs. obround cross-sectional profile. Both capillaries have the same flow area; however, the obround cross-section reduces max particle distance by approximately 20%

4.2.2 Plan of Action

Multiple methods to modify the capillary cross-section are considered. One way to achieve uniform heating within the capillary is to introduce a webbed structure or frit to the ID. This structure, which could be achieved by porous metal 3D printing, would increase conductive heat transfer to the center of the flow. However, this process is expensive, and the extra material may also increase ion losses to the capillary.

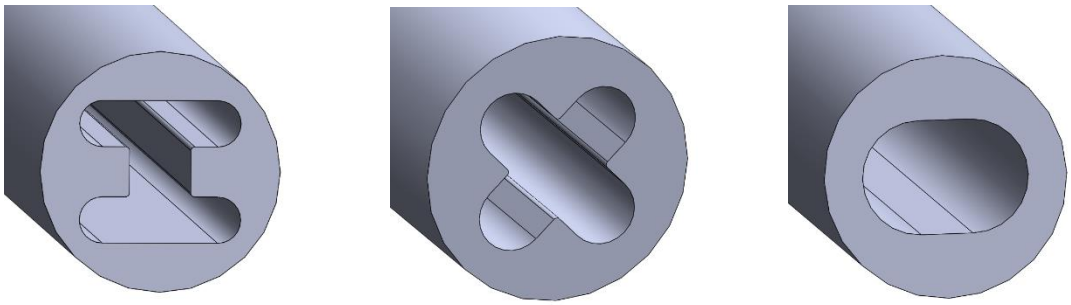

Figure 12: Various Capillary Cross-Sectional Profiles

Another method involves machining a capillary with a circular cross-section. The cross-section designs in Figure 12 can be fabricated in a few ways, including a wire EDM drilling process [24]. The Waters machine has wire EDM drilling capability. Machining these designs, with limits on minimum bore diameter, is possible. The minimum bore diameter possible through the machine shop is .016”, which is derived from the thinnest EDM drills they have.

The final and chosen method of modifying the cross-section was purchasing existing capillaries with non-standard cross-sections. Specifically, multi-channel wire EDM drills were used for this experiment due to a variety of configurations, low procurement time, and low cost. Multi-channel drills are used for wire EDM as they will remove excess material from the center of the drilling operation, unlike single-channel drills. The channels carry dielectric fluid to the workpiece, which sparks when a voltage is applied to the drill. These sparks wear away at the

workpiece, carrying out the drilling process. These drills are manufactured through a cold drawing process, with the inner channels being compressed within a larger outer tube. Materials typically used to make these drills are brass, copper, tungsten, and graphite. Although they are meant to carry dielectric fluid, they can be used to carry entrenched ions to the MS in this experiment.

There are four types of commonly used wire EDM drill cross-sections (Figure 13). These cross-sections were acquired, imaged on a Starrett video microscope, and modeled in SolidWorks CAD. The drills, to be addressed as capillaries moving forward, have a .0787” OD. This OD was used as it closely matched the .049”-SST capillary OD, enabling the use of the same setup between both the inner diameter and cross-sectional profile experiments.

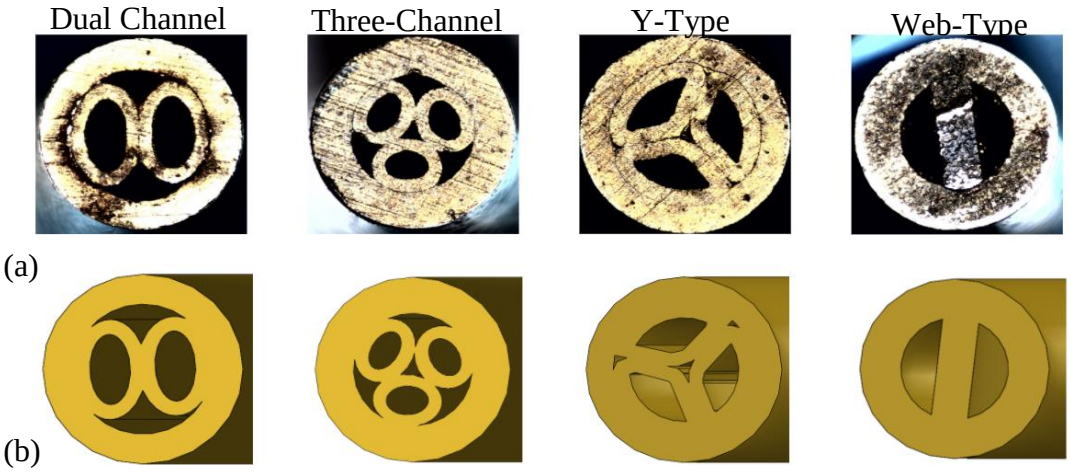

Figure 13: (a) Wire EDM Drill Cross-Sectional Profiles (b) Profiles modeled in CAD

With the known OD, other parameters such as flow area and max particle distance from a wall were extracted (Table 2). The flow area of the brass capillaries is 30-50% smaller than the .049”-SST capillary; however, the max particle distance from a wall is 80- 85% shorter on average.

Table 2: Wire EDM drill characteristics. .049"-SST characteristics included for comparison

	Dual-Channel (Plugged)	**Three Channel (Plugged)**	**Y-Type (Plugged)**	**Web-Type**	**Current Capillary .049"-SST**
Outer Diameter (10^{-2} in.)	7.87	7.87	7.87	7.87	8.30
Flow Area (10^{-3} in.^{2})	1.21 (0.737)	.828 (0.473)	.827 (0.786)	.902	1.89
Max Particle Dist. from Wall (10^{-2} in.)	.802	.615	.691	.748	4.15
Number of Channels	4 (2)	7 (3)	6 (3)	2	1

4.2.3 Brass Capillary Challenges

A few concerns exist with the brass capillaries. The first concern is the smaller overall flow area when compared to the .049"-SST capillary. The reduced flow area may cause decreased signal intensity as the capillaries may capture less of the ions. To alleviate the potential effect on the results, the .039"-SST capillary is used to make a better comparison between the circular and the multi-channel cross-sectional profiles. The 039"-SST capillary has a smaller flow area of 1.19E-3 in.^{2}, which is still slightly larger than some of the profiles.

The second concern is the side channels (Figure 14). These side channels have a flow area that differs from the main channels; this will introduce variability within the flow of the ions. A potential solution to this is plugging up the inlet end of these channels with Torr Seal epoxy, generally used to seal vacuum leaks. However, this magnifies concern #1, as the flow area is further diminished. In order to keep the flow area in the brass capillaries as large as possible, the

side channels are kept; however, their contribution to signal intensity may be negligible or even harmful.

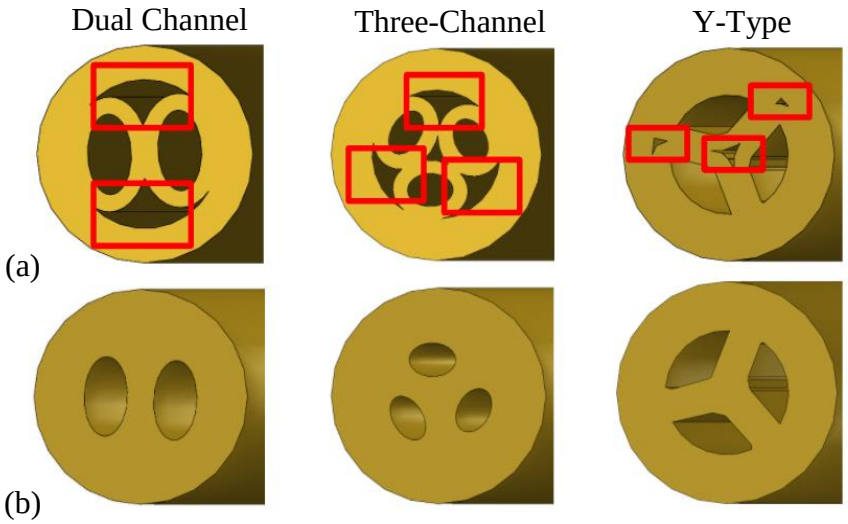

Figure 14: (a) The brass capillaries have side channels with a different profile than the main channels. These channels introduce flow variability due to the differing area. (b) Plugged versions of the brass capillaries

The final concern revolves around the material. Brass is a softer metal than the SST alloys and Inconel. The melting point is much lower than the other materials, shown in Table 3, which may pose a problem as the capillaries may start to soften and sag under high temperatures. The thermal conductivity is also far higher; however, thermal modeling indicates there is virtually no difference between brass and 304SST on capillary inner wall temperature (Figure 15). These brass capillaries may be acceptable for this set of experiments, but the long-term will require a switch to a material with a higher melting point.

Table 3: Properties of different capillary materials, including the material used for the nose cone

	304SST [25]	Inconel 600 [26]	Brass 63/37 [27]	316SST (Nose Cone) [28]
Yield Strength (MPa)	215	310	315	290
Thermal Conductivity (W/m.K)	16.2	14.8	120	16.3
CTE at 20°C (µm/m-°C)	17.3	13.3	19.9	16
Melting Point (°C)	1400-1455	1354- 1413	915- 955	1370- 1400

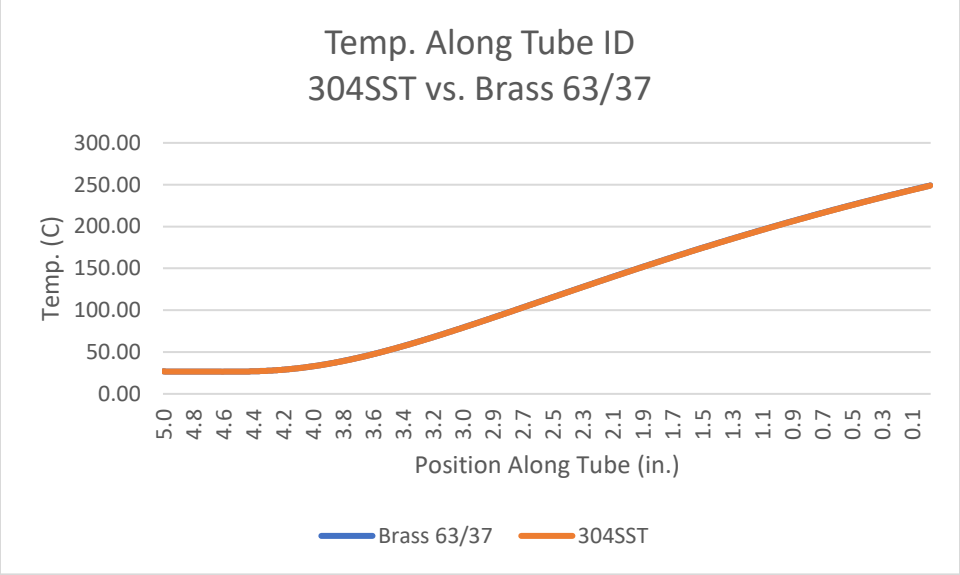

Figure 15: Temperature along inner wall for 304SST and Brass 63/37 [23]

4.3 Selected Temperatures

The signal intensity provided by the capillaries is evaluated at four temperatures, ambient, 100˚C, 200˚C, and 300˚C. Prior experiments have heated the capillaries up to 450˚C [21]. However, this poses two problems. First, heating the capillary to too high of a temperature may cause fragmentation of molecules. Fragmentation of molecules involves them breaking apart from the standard *m/z* into smaller *m/z*, which can be detected from the changing peaks of the mass spectrum. Since testing for fragmentation is not a goal of this experiment, heating to such high temperatures is not necessary. Second, the brass is a softer material than the standard SST, as previously discussed. The brass capillaries will not be heated to temperatures higher than 300˚C to limit sag. To draw a better comparison between all capillaries, the same range of temperatures are tested.

Although there is a potential to evaluate the capillaries at higher temperatures, the selected ambient to 300˚C range should provide enough data to understand changes in heating efficiency. In previous research, heating from ambient temperature to 300˚C has provided a few magnitudes of increase in signal intensity. The jump in signal intensity from 300˚C to 400˚C was far smaller, partially due to fragmentation [21]. Based on our hypotheses for the experiment, the brass capillaries and the smaller inner diameter capillary should be able to see a large increase in signal intensity from ambient to 300˚C due to increased ion desolvation.

CHAPTER 5

EXPERIMENT SETUP

In this chapter, the various steps performed to set up the experiment, including modifications to existing components and capillary assembly, are described.

5.1 Nose Cone Modifications

5.1.1 Nose Cone Overview

The nose cone is a component that connects the ion transfer capillary to the ion source (Figure 16). Typically, the capillaries are welded to the nose cone. However, this experiment involves a variety of capillaries, and the number of nose cones available is limited. Thus, modifications were made to the nose cone to allow swapping between different capillaries.

(a) (b)

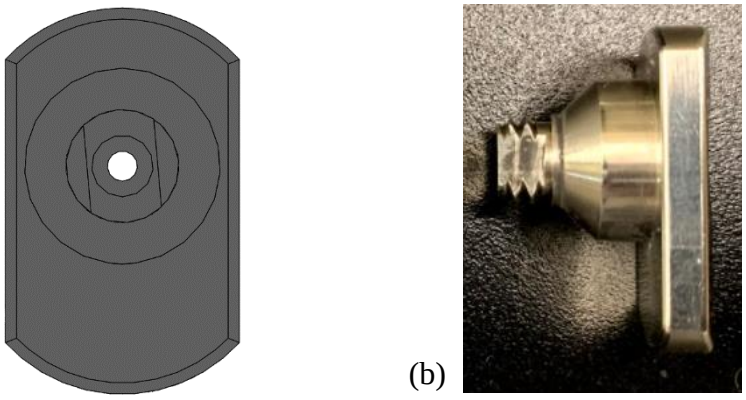

Figure 16:(a) CAD model of modified nose cone. (b) Side view of modified 316-SST nose cone.

5.1.2 Nose Cone Attachment Options

Two separate attachment options are designed. In both options, modifications to the nose cone include reducing the length of the inlet and threading the inlet.

Attachment option #1 features a nose cone adapter piece that threads onto the nose cone (Figure 17). The capillary fits inside the nose cone adapter and can slide into the nose cone inlet. Every time a capillary is swapped, a fixture is used to position the tube within the nose cone. A Viton O-ring is used to seal the space between the nose cone and the nose cone adapter. The nose cone adapter is designed to compress the O-ring by 20%. This compression also holds the capillary in place. The nose cone adapter is a novel design, and thus it would have to be machined from scratch.

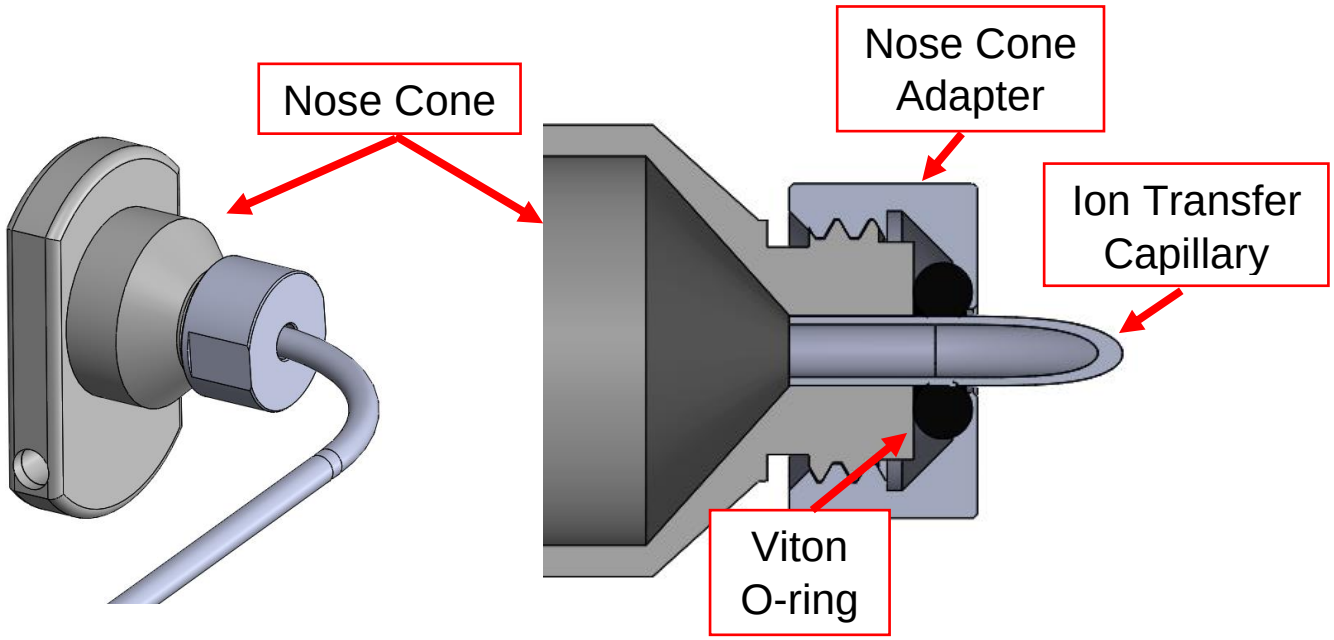

Figure 17: Attachment Option #1- Nose Cone Adapter

Attachment option #2 involves a Swagelok fitting (Figure 18). A Swagelok fitting uses ferrules to bite onto the ion transfer capillary. After tightening the assembly for the first time, the front ferrule sets onto the capillary. As a result, every time the capillary is placed back into the nose cone, its position relative position is the same. Tightening the nut also holds the capillary angle in place. Due to these positioning advantages and ease of procurement, this option is selected. However, a few modifications were required to make them compatible with this design. The nut,

front ferrule, and back ferrule, available in .0787” ID, all had to be reamed to a larger OD to fit the .083” OD capillaries. The nose cone inlet also had to be countersunk to allow the front ferrule to form a seal. The countersink angle had to be estimated from existing Swagelok fittings and scaled to this ferrule’s geometry, as this information was not publicly available. The fitting was tested for leaks in a water bath, and no significant leaks were detected. This design is carried forward into the experiment.

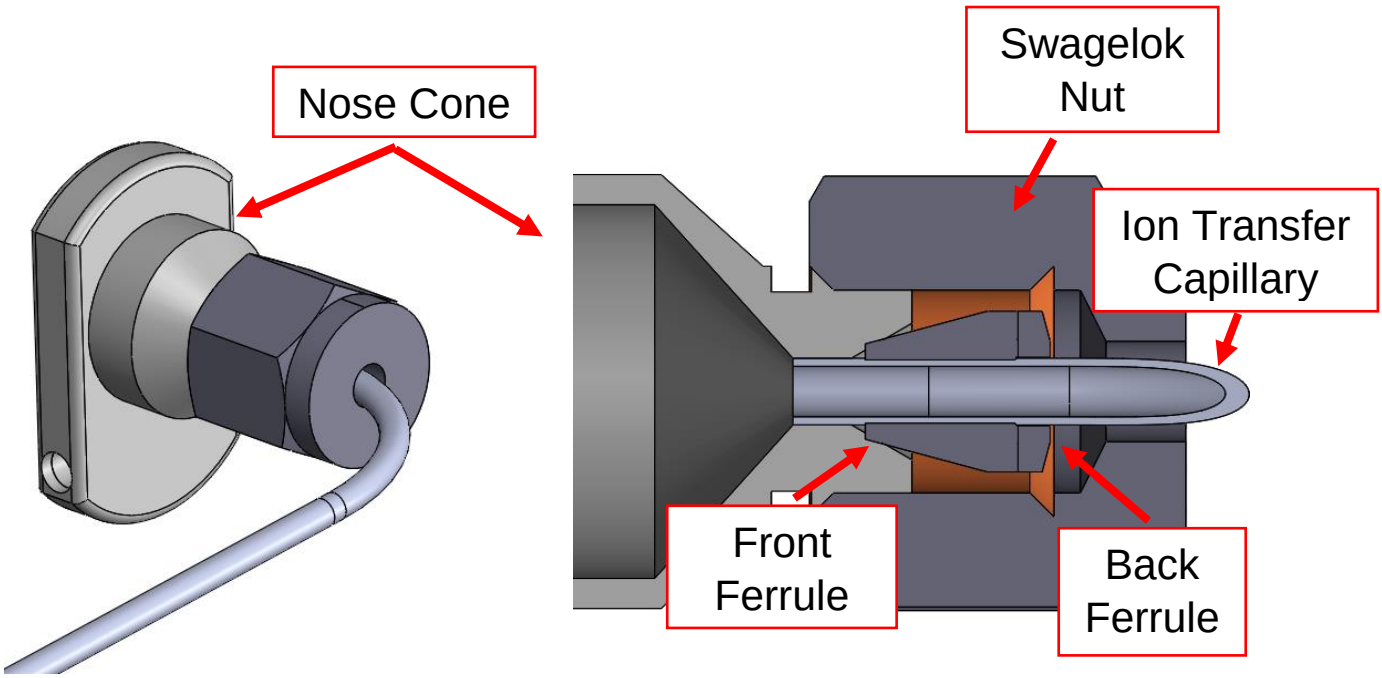

Figure 18: Attachment Option #2: Nose Cone Swagelok Fitting

5.2 Fixturing

Fixtures to assemble the capillary to the nose cone are necessary to produce assemblies with little to no variation in dimensional accuracy. Four key steps in the assembly process require the use of fixtures. The first fixture must hold the capillary in place within the nose cone inlet when tightening the Swagelok fitting. This fixture must ensure all capillaries are located at the position within the nose cone inlet. The second fixture is the bending fixture. The capillaries must all be

bent to the same 90˚ angle. Next, the capillary angle must be held at 5˚ (Figure 19). The capillary angle fixture must hold the capillary at this angle while tightening the Swagelok nut. Finally, the heater must be attached 1.5” from the inlet of the capillary.

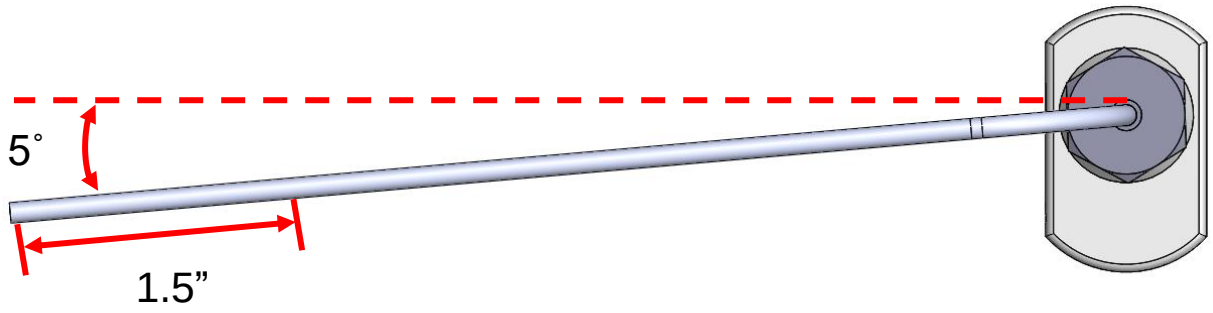

Figure 19: Capillary must be held at 5˚ angle, and the heater must be attached 1.5" from the inlet

The fixtures are rapidly prototyped using SLA 3D printing. After an iterative design process, a final fixture is created that incorporated all these steps into one component (Figure 20). This fixture includes mounting holes for mounting to a more stable surface, as well as thumb holds for better grip. The whole capillary-to-nose cone assembly process can be completed with this one fixture.

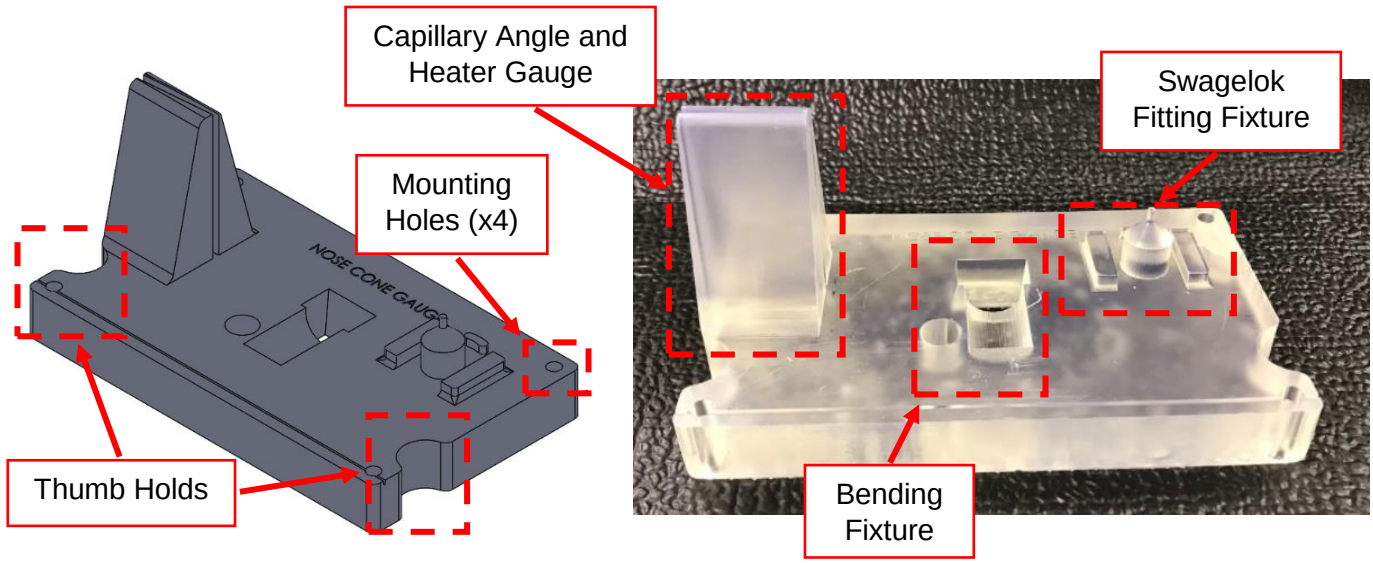

Figure 20: Final capillary assembly fixture, including the CAD model and 3D printed part. Bending fixture handle not shown.

5.3 Capillary Assembly

The next step in the experimental setup is assembling the capillaries (Figure 21). The procedure for making the brass and SST capillaries experiment-ready is as follows.

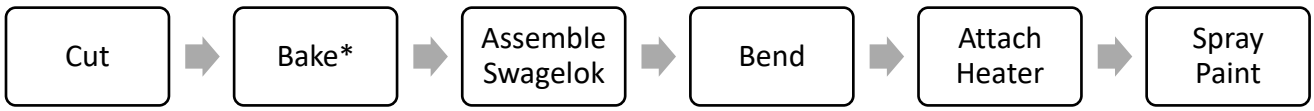

*only for brass capillaries

Figure 21: Capillary Assembly Process

5.3.1 Cutting

The capillaries must first be cut to the standard length of 5.17”. This length ensures the capillary inlet reaches the optimal position above the sample. Wire EDM is used to cut the brass capillaries down to size. Standard cutting techniques such as a miniature saw closed off portions of the capillary. Wire EDM provided the capillaries with a clean finish at the inlet and outlet. The

SST capillaries did not face the same problem being cut with a miniature saw as they had a circular cross-section; however, deburring is required. A fixture to hold the capillaries steady and ensure flat surface profile while sanding was made from PEEK. Although all capillaries were wire EDM cut to length, the sanding fixture allowed for some post-processing on the capillary finish.

5.3.2 Baking (only for brass capillaries)

One problem that presented itself arose from the composition of brass. Brass is a copper and zinc alloy, with the alloy in capillaries containing nearly 37% zinc. Zinc has a relatively high vapor pressure when heated under a vacuum (Figure 22). The zinc can deposit in the MS while using the heated brass capillaries, potentially compromising the system.

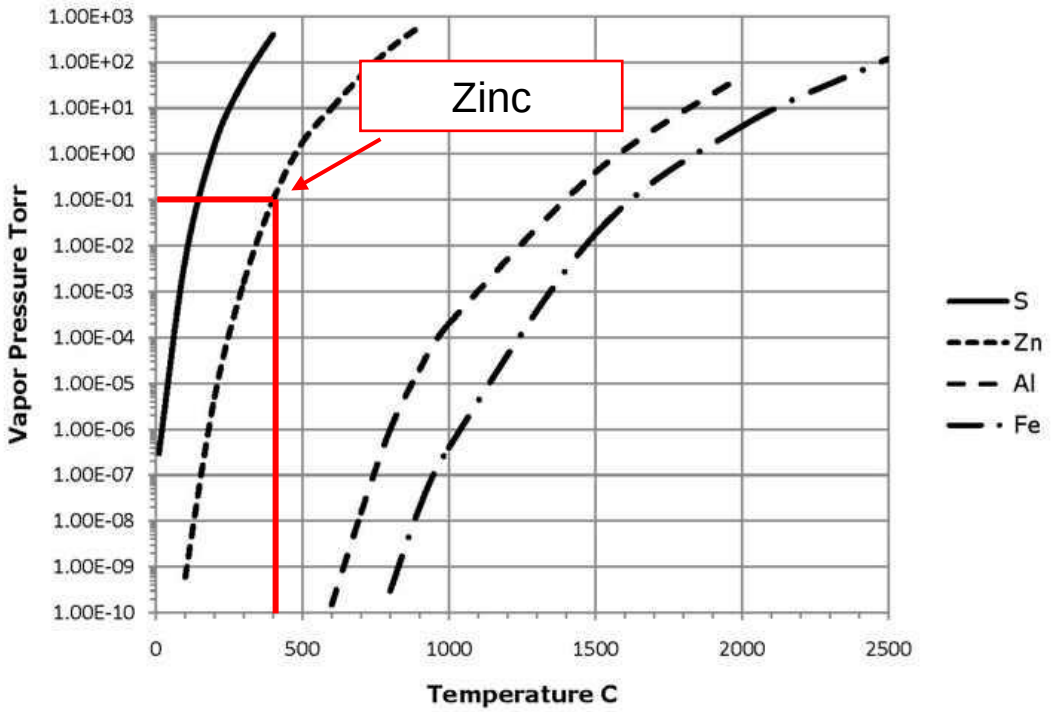

Figure 22: Vapor Pressure of Select Elements as Function of Temperature [29]

Two solutions are developed to alleviate this issue. The first, short-term solution is to bake the capillaries for a long time at high temperature. The mass before and after baking the capillaries at 310˚C for 18 hours was measured; virtually no change in mass was detected (Table 4). The caveat

here is that the baking process did not take place under a vacuum. However, due to short testing times, these capillaries were used for testing. The second, long-term solution is to use wire EDM drills made of copper as capillaries, as they contain no zinc.

Table 4: Mass of Brass Capillaries Before and After Baking

Cross Section	Weight x3 (g)	Weight x1 (g)
Before Baking		
Y-type	8.5981	2.8660
Web-type	8.5339	2.8444
Dual Channel	7.6514	2.5505
Three Channel	8.7400	2.9133
After Baking		
Y-type	8.5981	2.8660
Web-type	8.5340	2.8447
Dual Channel	7.6499	2.5500
Three Channel	8.7405	2.9135

5.3.3 Assembling Swagelok

After being cut to length and, if necessary, baking, the capillaries are ready to be fitted with a Swagelok. The Swagelok fitting fixture sets the capillary position in the nose cone inlet, and then the nut is tightened, putting the ferrule in place (Figure 23).

(a)

(b)

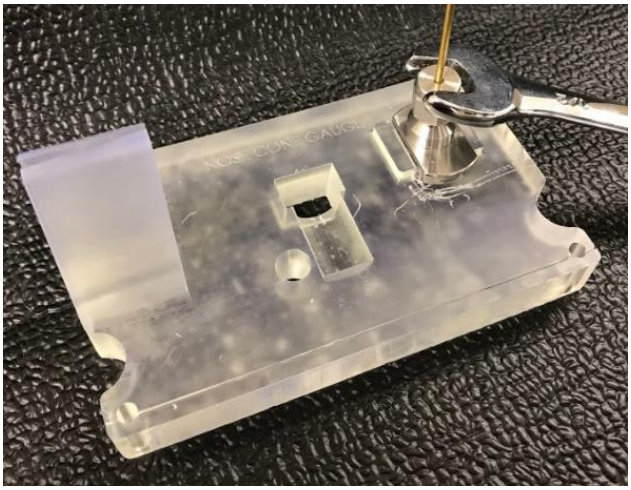

Figure 23: (a) Mount Swagelok components to capillary and (b) tighten on Swagelok fitting fixture

5.3.4 Bending

After being cut to length and, if necessary, baking, the capillaries are ready to be bent. The capillaries must be bent to a 90˚ angle as the nose cone is mounted perpendicular to the sample stage, as seen in Figure 7. The experimental capillaries have the same bend profile as the existing capillaries. Figure 24 describes the bending process.

(a) 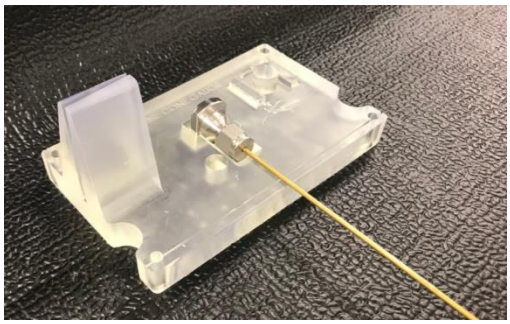 (b) 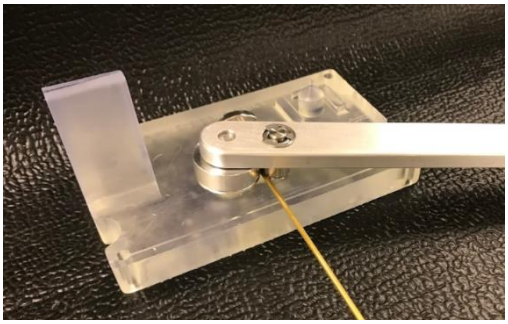

(c) 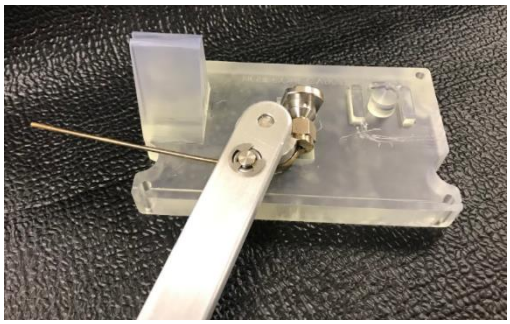 (d) 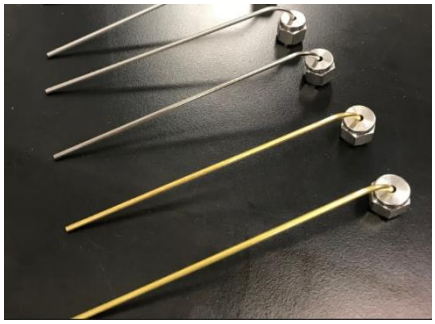

Figure 24: Capillary bending procedure. (a) Insert nose cone and capillary assembly. (b) Insert capillary into bending fixture handle. (c) Bend capillary to 90˚. (d) Capillaries after bending.

5.3.5 Attaching the Heater

Multiple methods for heating the capillary are taken into consideration, including cartridge heaters, resistive heating, and a nichrome rope wire heater. The nichrome rope wire heater option is selected due to ease of installation and effectiveness at bringing the capillary up to temperature (Figure 25). The nichrome rope wire heater is rated for 48V and 70W and is 17.25” long. The rope wire heater is tightly coiled around the capillary. After coiling, the heater is positioned 1.5” from the inlet with the use of the capillary assembly fixture. The inlet end is tied off tightly with Inconel wire. Molex connectors are crimped to the ends of the rope wire heater to connect to a power supply quickly. Finally, a zip tie is used to hold the insulated wires together.

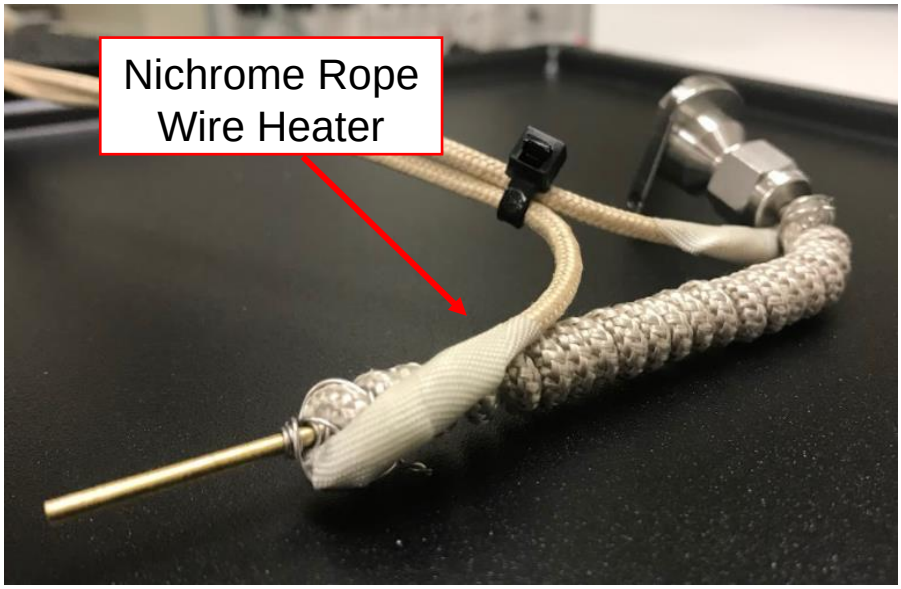

Figure 25: Capillary with Heater Attached

5.3.6 Spray Painting

In the final step of the process, the capillary end is sprayed with high-heat resistant black paint (Figure 26). This step is essential as the thermal camera used to monitor the system will not be able to measure the temperature of the metal surface accurately. The black paint will increase the emissivity of the heated capillary and improve the accuracy of the temperature profile.

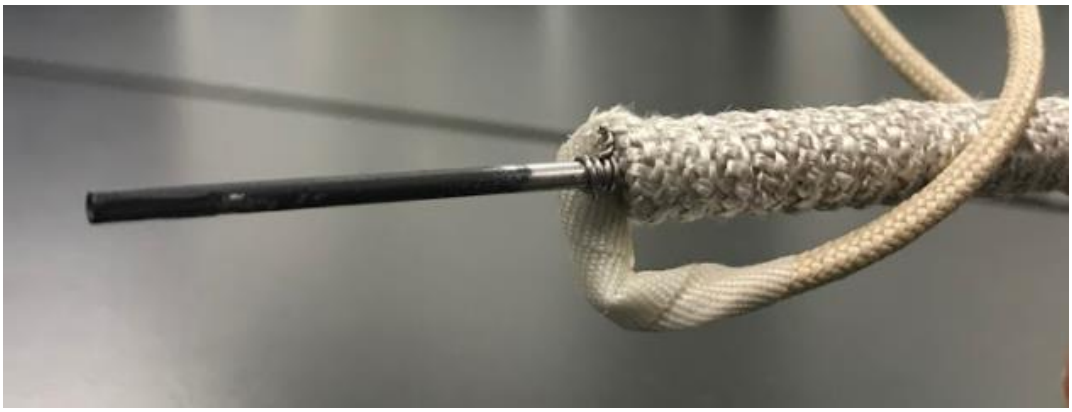

Figure 26: Spray painted and fully assembled capillary

5.4 System Components

Figure 27 shows the full experiment on the SYNAPT G2-Si HDMS, with key components labeled. The power supply unit will be used to supply the rope wire heater. The voltage and current are set to bring the capillary up to the desired temperature, which will be monitored by a thermocouple sensor. A thermal camera mounted above will also be used to monitor the temperature along the outer profile of the capillary. The Dino-lite Digital Microscope will monitor the capillary and sprayer position. The syringe pump will provide the solvent to the sprayer. The MS operating system and the camera operating system will be used to operate the MS and the cameras.

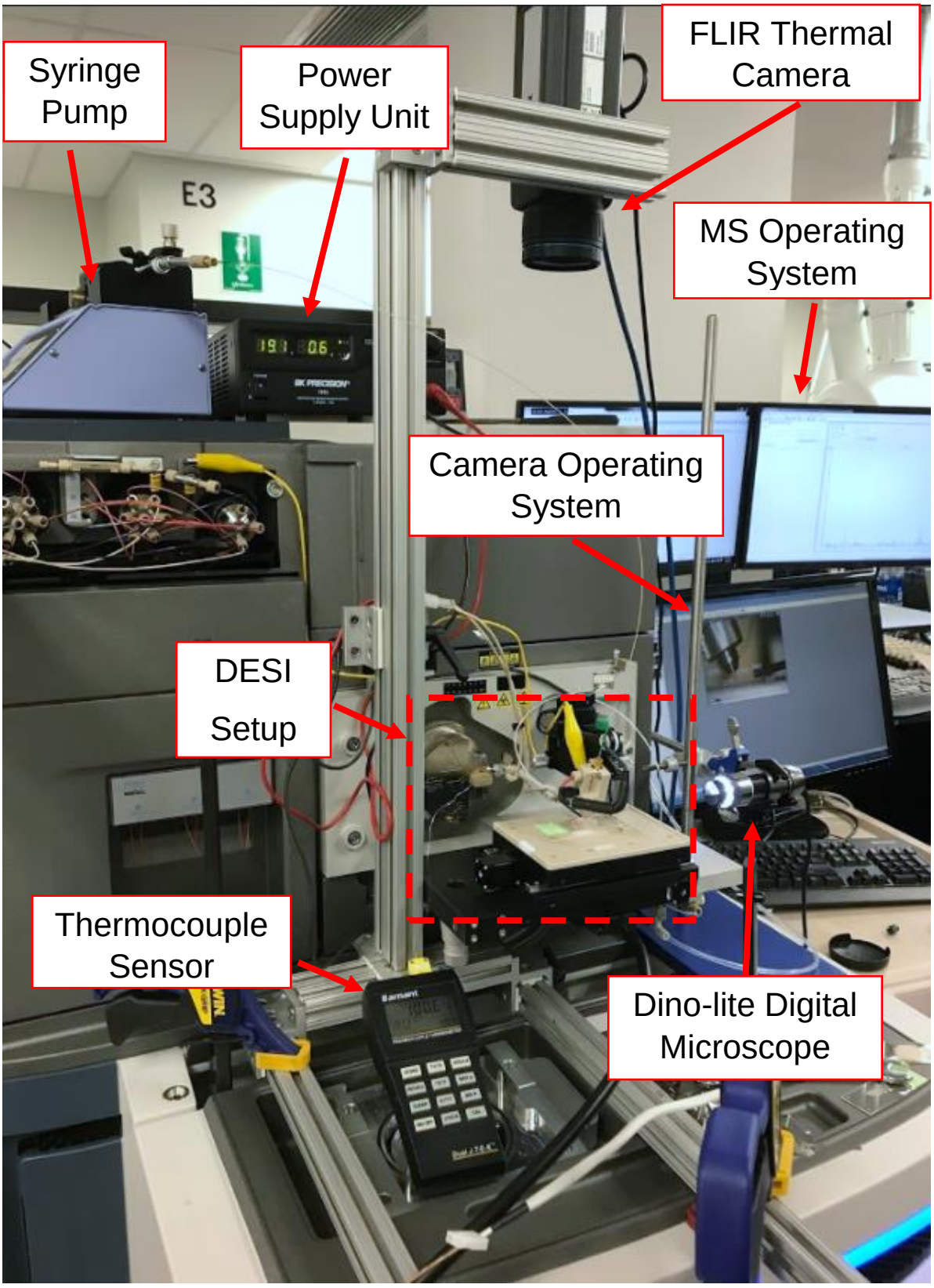

Figure 27: Full experiment setup with the key components labeled.

CHAPTER 6

EXPERIMENTAL PROCEDURE

This chapter discusses the experimental procedure in detail, as well as potential sources of variation. Figure 28 displays the general workflow diagram.

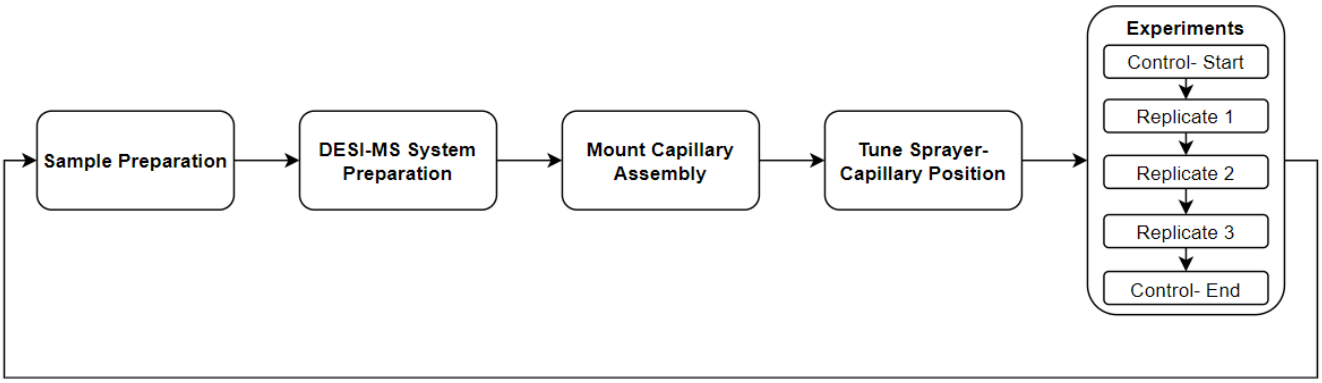

Figure 28: General procedure for the experiment. Repeat for all capillaries.

6.1 Sample Preparation

Pig liver is the choice of sample that is used throughout all the experiments. Homogeneity is the primary quality that is desired in choosing a suitable sample for the experiment. Pig liver is a relatively homogenous biological sample that has a known *m/z* of 885. Fully homogenous solutions with known *m/z* could be made; however, these solutions would not be representative of actual biological samples.

The pig liver is kept in a Leica CM3050 S cryostat (Figure 29). A microtome within the cryostat thinly slices the pig liver into sections ~15 microns in thickness. A few sections are sliced

off to ensure the experiment sample is fresh. The slice is transferred to a slide and is ready to be used. The procedure is as listed below.

1. Slice off sections of pig liver sample until a fresh section is revealed
2. Close the glass pane on top of the stage
3. Carefully slice the sample once, ensuring the sample is not overlapping
4. Open the glass pane and place the clean slide on the sample
5. Let sample adhere to slide

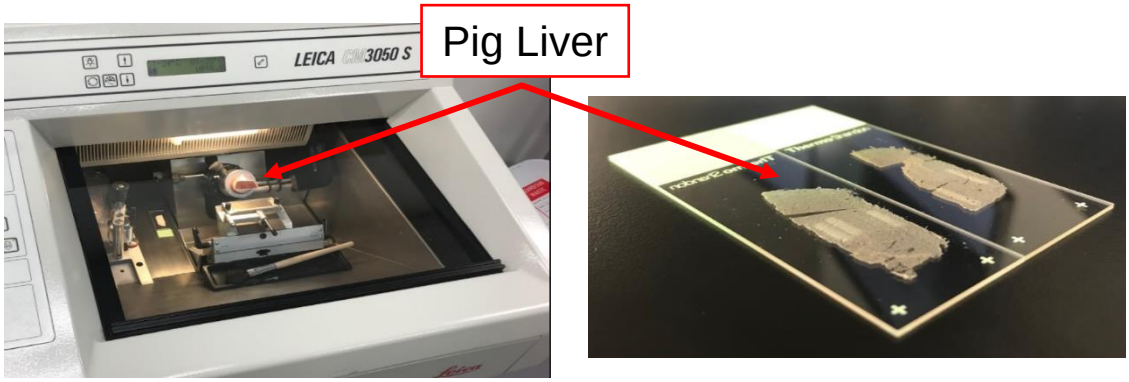

(a) (b)

Figure 29: (a) Pig liver sample in cryostat. (b) Sliced pig liver sample with a ~15-micron thickness.

6.2 DESI-MS System Preparation

Once the sample is prepared, the DESI-MS system must be setup. The detailed procedure is as follows.

6.2.1 Software Setup

The first step is loading an image onto the MS operating system and setting up the software. The procedure is as follows.

1. Load image of sample onto HDI Methods Software

2. In the “Acquire” tab select
    a. Target Instrument: SYNAPT
    b. Experiment Type: DESI-MS
    c. Start Mass (*m/z*): 50
    d. End Mass (*m/z*): 1200
    e. Trap Collision Energy: 4
    f. Transfer Collision Energy: 2
    g. Polarity: Negative
3. In the “Pattern” Tab, draw the area to be analyzed by the MS (Figure 30)
    a. Select a 10mm by 1mm area
4. Choose pixel size of 50µm x 50µm
5. Select a scan rate of 500µm/s
6. Save .pdm file and export to MassLynx to generate a .raw file
7. Open MassLynx and open .raw file. Experiment is now ready to run.

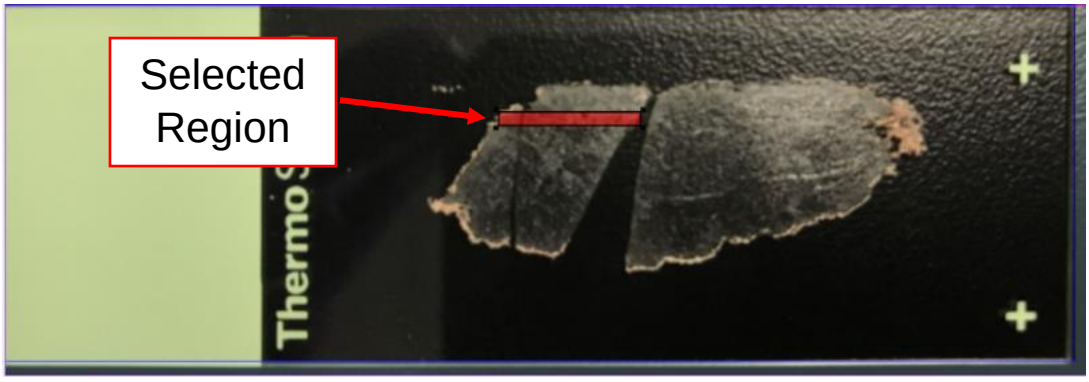

Figure 30: Selected region to be analyzed by the MS as drawn on HDI methods software

6.2.2 DESI Sprayer Setup

1. Ensure sprayer nozzle is clean; if not, clean with IPA
2. Start infusion flow from Harvard Apparatus Syringe Pump; if empty, refill with 98% MeOH solution
    a. Flow Rate: 5µl/s
3. Plugin sprayer power line to MS; this provides the voltage to the sprayer
4. Wait for flow to reach sprayer (~10 min); check MS to see if there is a strong signal

6.3 Experimental Procedure

6.3.1 Mounting Capillary Assembly to MS

Every time a new capillary is to be tested, it must be mounted to the MS. The procedure is as follows.

1. Turn off flow to MS and remove the old capillary from the MS
2. Swap the old capillary on the nose cone to the new capillary
    a. Use capillary fixture assembly to tighten Swagelok fitting
3. Ensure flow restrictor cone is still in place within the nose cone and clean assembly with IPA (Figure 31)
4. Place capillary assembly back in MS and ensure nose cone is flush with the ion source
5. Insert thermocouple wire between rope wire heater and capillary
6. Turn on flow to MS. Capillary is now mounted.

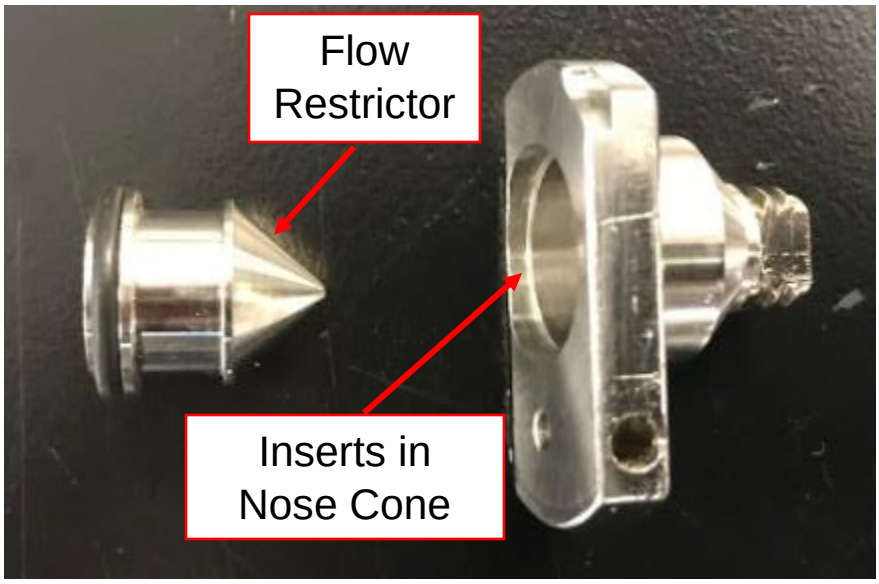

Figure 31: Flow restrictor inserts into the nose cone

6.3.2 Capillary- Sprayer Optimization

The position of the capillary relative to the sprayer and the sample is a vital parameter. Small changes in position can have large effects on the signal intensity of the experiment. Thus, every time a capillary is mounted for the first time, its position and the sprayer position are tuned. A Dino-lite Digital Microscope is used to monitor the sprayer and capillary position during the experiment (Figure 32). Once tuned for the first time, the critical dimensions of the sprayer and capillary positions are saved for each capillary type (Figure 33). These dimensions are used to ensure a consistent position through all experiments.

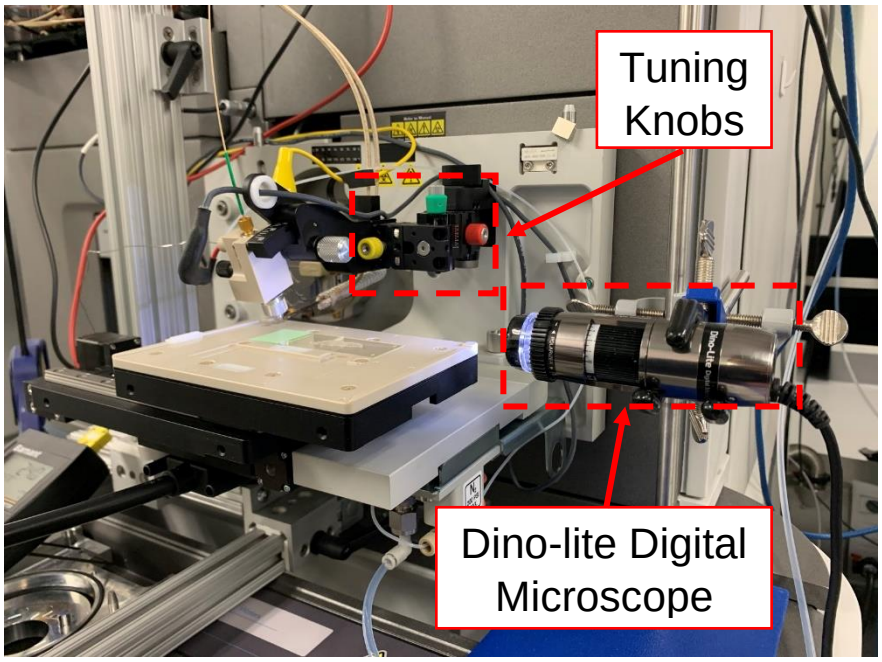

Figure 32: Dino-lite Digital Microscope setup to monitor position of capillary and sprayer, as well as knobs to tune sprayer- capillary position

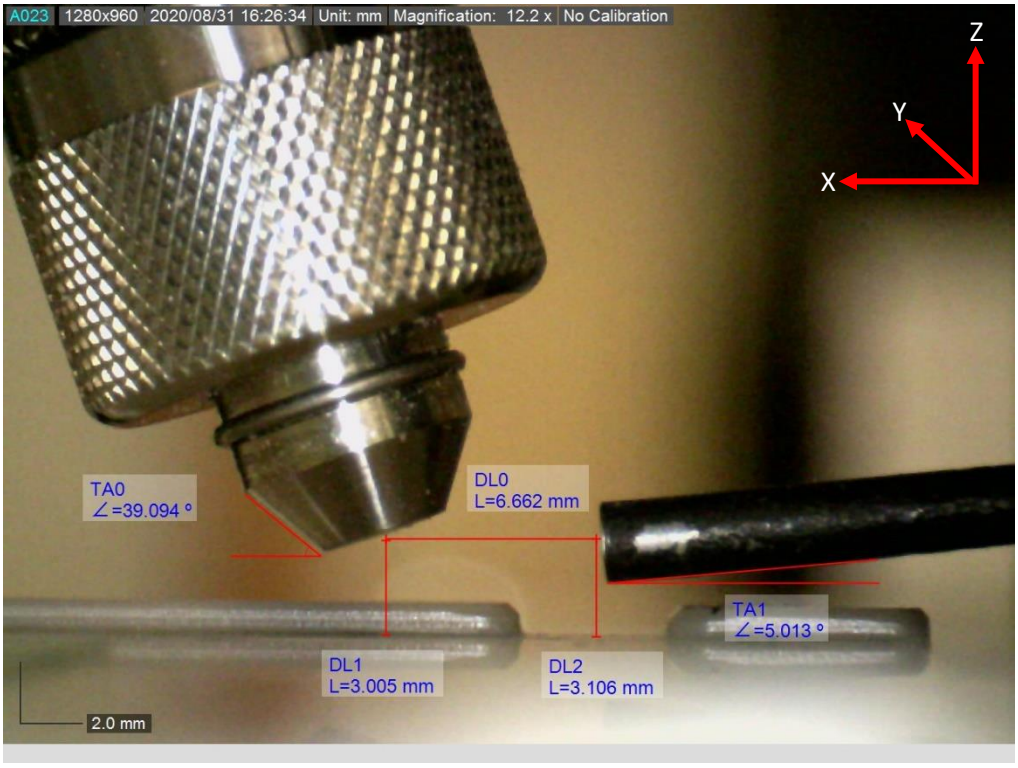

Figure 33: Position of sprayer and capillary as captured by the Dino-lite Digital Microscope, with a coordinate frame defined on the top right

The tuning procedure is as follows:

1. Disconnect DESI Source Control in SYNAPT menu
2. In SYNAPT → Acquire → create .raw file
    a. Select range of m/z (800 to 900)
    b. Select scan time of 1 sec
3. In MassLynx, open chromatogram and select tuning .raw file
    a. Activate clock function to see MS output in real-time
4. Open OmniSpray
5. Jog along sample and adjust knobs in the order of: green → red → yellow (Figure 32)
    a. Green: Changes position of sprayer in z-axis
    b. Red: Changes position of capillary in x- axis
    c. Yellow: Changes position of capillary in y- axis
6. Look for intensity peaks in chromatogram, tune until intensity plateau is reached

6.3.3 Running the Experiment

Each experiment consists of one control at the start of the experiment, three replicates, and one control at the end of the experiment. The controls are run at ambient temperature. The three replicates are run at the temperature required for the experiment, which are either ambient, 100˚C, 200˚C, and 300˚C.

During the experiment, the sample stage moves in the *x* and *y*-axis such that the desired sample area is analyzed. The sprayer emits the plume of solvent towards the sample and ionizes the molecules, as described in Chapter 3. The procedure for the experiment is as follows.

1. Ensure capillary is in an optimized position, sample is in place, and signal to MS is strong

2. Open .raw files in MassLynx → select control start file→ check and record thermocouple temperature → run control start experiment
3. Once acquisition stops, proceed to select replicate file→ bring capillary up to the required temperature using PSU and thermocouple→ record temperature, voltage, and current→ turn on FLIR thermal camera→ run the replicate experiment
4. Repeat step 3 for all replicates. Ensure temperature and capillary position stay consistent
5. After replicate experiments, turn of PSU → let capillary return to ambient temperature → run control end experiment

6.4 Sources of Variation

Sources of variation are important to ensure collected experiment data is reliable. Without addressing sources of variations, flawed conclusions may be drawn from the data. This experiment contains four main sources of variation, including sprayer parameter variation, sample-to-sample variation, within-sample variation, and finally, between capillary variation.

6.4.1 Sprayer Parameter Variation

Small changes to sprayer position can result in a large drop in signal intensity. Sprayer parameter variation is addressed in two ways. First, every time a capillary is mounted for the first time, the tuning procedure described in section 6.3.2 is executed. The optimal position of each capillary is captured with the Dino-lite Digital Microscope. The position of the capillary is monitored throughout the experiments and reset if necessary.

6.4.2 Within Sample Variation

Within- sample variation encompasses the variation that occurs due to inconsistencies in spatial sample distribution. The pig liver is considered a homogenous sample for MS analysis; however, variations within sections of the sample still exist (Figure 34). In addition, the freshness

of the sample also plays a role in the acquired signal intensity, as a dry sample may not ionize to the same degree as a fresh sample. Each sample is used for approximately one hour, the length it takes to go through a single temperature- capillary combination. The grand control at the beginning of each type of experiment, which consists of 5 runs at ambient temperature, is used to characterize within-sample variation.

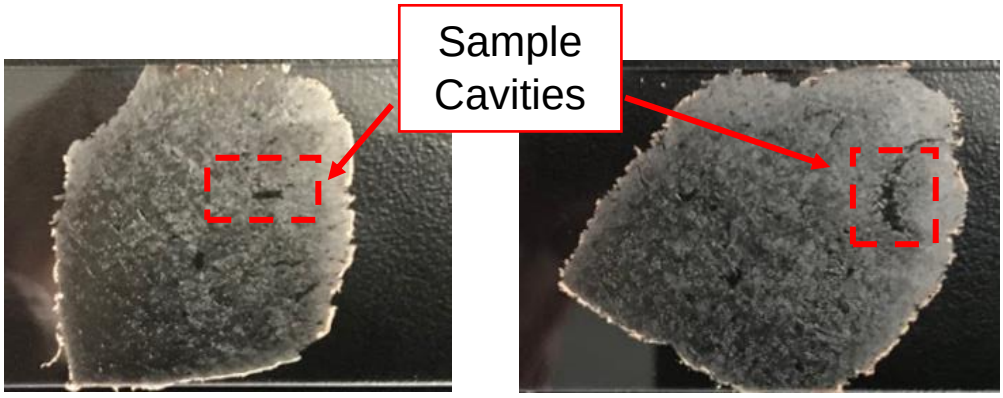

Figure 34: Cavities within the sample produce within-sample variation. The distribution of these cavities are random from sample- to- sample, another source of variation.

6.4.3 Sample- to- Sample Variation

The cavities that occur in the sample are randomly distributed and change from slice to slice (Figure 34). As a result, no two samples are the same. When setting up the experiment, care is taken to image areas without large cavities; however, variation will still be present. In addition, changes in the environment may also affect the signal intensity of the MS. The control at the beginning and end of each capillary- temperature combination will be used to ensure there are no significant changes between each sample.

6.4.3 Between Capillary Variation

In any manufacturing process, no two parts produced are exactly alike. This holds true for these capillaries. Variations exist, such as different surface roughness and differing channel

dimensions. Although these are small, they still play a role in a capillary's effectiveness at transferring ions. Ideally, multiple capillaries from each selected ID and each cross-section would be tested to characterize this source of variation. However, due to time constraints on the experiment, this source of variation is not characterized.

CHAPTER 7

DATA ACQUISITION AND ANALYSIS

7.1 Data Acquisition

The first step of acquiring the data is to upload the .raw files into the HDI methods software. HDI processes the .raw file by scanning each pixel in the sampled area. The mass spectra of each pixel are determined. From this data, intensities for various *m/z* can be visualized in the analysis tab of the software. From here, the data can also be exported to a file format known as imzML. imzML is a data format that is developed for efficient storage and processing of mass spectrometry data [30]. Once exported, these files can be used in other software for post-processing and analysis.

7.2 Data Analysis

This section describes the tools and methods used to analyze the MS data. The full code is found in the APPENDIX.

7.2.1 Data Processing Tools

Once exported to an imzML file, the data will be processed in R, a data analysis software. Cardinal 2 is an analysis library in R that is used primarily for processing data from MS experiments [31]. This library is used in R to understand mass spectra data for each experiment fully. This library is important as the data collected in these MS experiments is extensive. Depending on the number of ions counted by the MS for each experiment, the associated size of the imzMl files can take up multiple gigabytes in computer storage. Cardinal can read imzML files and efficiently stores and recalls the MS data in memory, lowering process times.

7.2.2 Data Format

The imzMl files are read in Cardinal using a method called *readMSI*. This method converts the file into a *MSProcessedImagingExperiment* object in R that contains the data regarding the MS experiment. The fundamental data structure in this object is the intensity matrix.

The intensity matrix contains mass spectrum data for every single pixel in the experiment (Figure 35). The size of this matrix is determined by the number of features and the number of pixels. The features are the values of the mass spectrum. In these experiments, data for ions within the 50- 1200 *m/z* range are collected; thus, the mass spectrum will be limited to this. The number of features depends on the resolution at which the mass spectrum values are binned. The number of pixels is defined during the experiment setup. In these experiments, each pixel covers a 50 x 50-micron area on the sample. Four thousand pixels are required to cover the 10mm x 1mm area imaging in each replicate.

Many operations can be performed on this intensity matrix. This includes summing the intensities across all the pixels, finding the average intensity, as well as finding the standard deviation of intensity data. Subsets of the matrix can also be created. For example, analysis for this experiment will take primarily in the 880- 890 *m/z* range, due to the pig liver's known 885 *m/z*. A subset for this mass range is created, such that each pixel's mass spectrum is limited to this range.

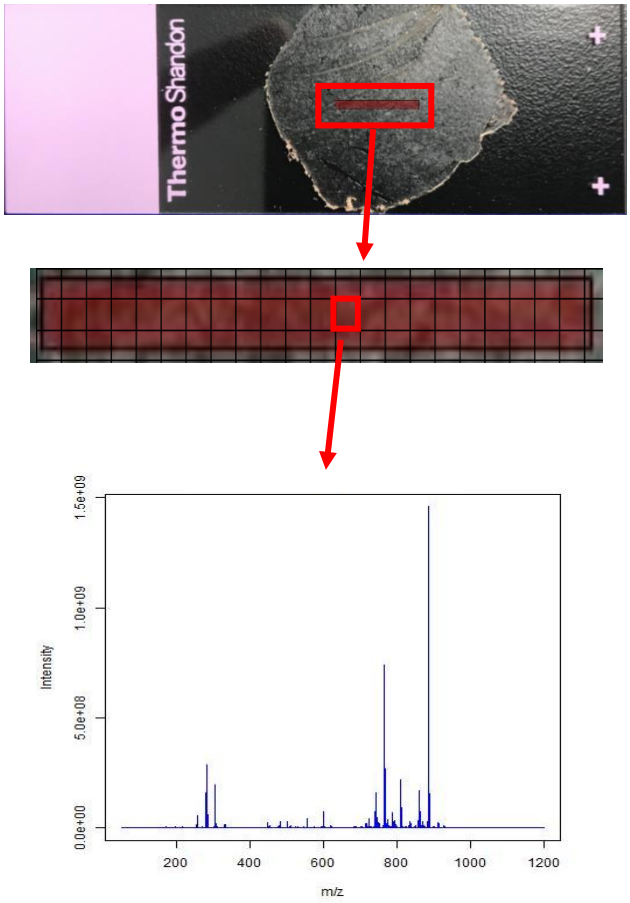

Figure 35: Format of data. The imaged sample area is broken up into pixels. The mass spectrum at each pixel creates an intensity matrix that can be used for processing.

7.2.3 Within Capillary Analysis

Analysis of all the experiments for each specific capillary type is performed first. The key data extracted for this analysis are total intensities, mean intensities, and standard deviation of intensities for the selected mass range of 880 – 890 *m/z*. This information is collected for each replicate within each set of temperature experiments. The purpose of this is to visualize how intensity is affected as the temperature is increased.

The control experiments for each set of temperature experiments are used to validate the data and characterize any sources of variation. Sample-to-sample variation is characterized by plotting the total intensity within the 880- 890 mass range at every single pixel for all control

experiments (Figure 36). The ambient temperature controls and replicates are treated as a grand control, and the sample size for that boxplot is 5. As previously discussed, the two controls for the elevated temperature experiments are also conducted at ambient conditions and provide information on sample and environment changes contributing to signal intensity.

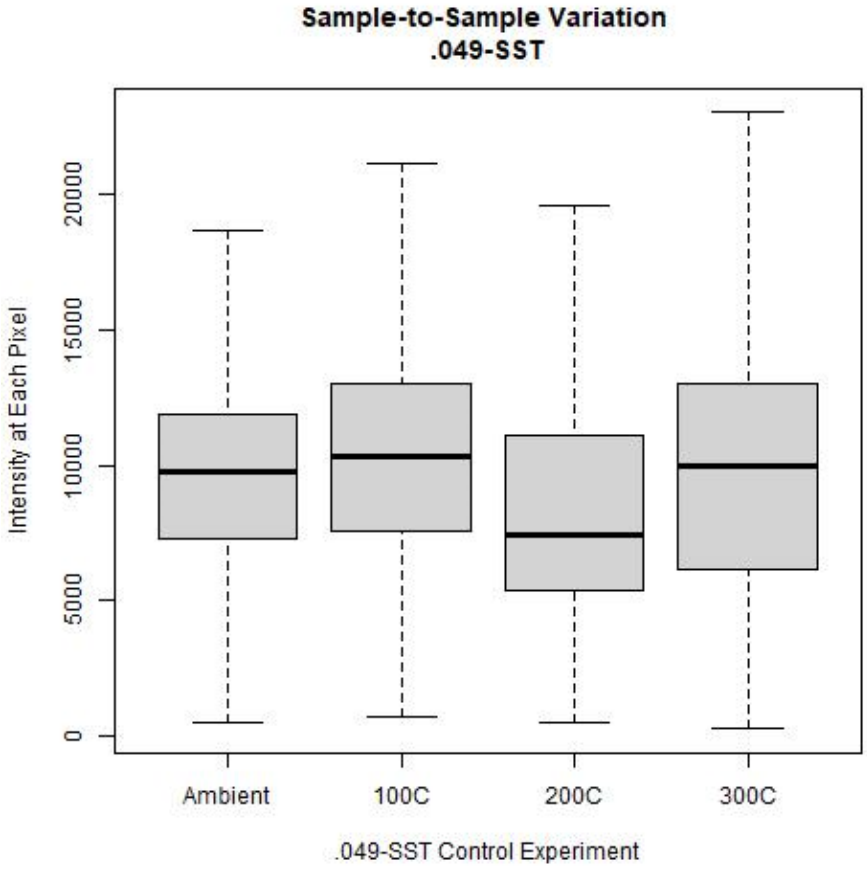

Figure 36: Sample- to sample variation is characterized by plotting the total intensity each pixel in a control experiment experiences within the 880- 890 m/z range. The sample size for the ambient control is five, as the two control experiments and three replicates are all run at ambient conditions. The sample size for the elevated temperature control experiments is two, one control at the start and one control at the end. In this example, the sample-to-sample variation is considered insignificant as all experiments median and IQR fall within each other's range.

Within- sample variation is characterized by plotting the mean intensity experienced within the 880- 890 mass range across all pixels in a single ambient control or replicate run (Figure 37). This variation essentially characterizes spatial variation within the sample and is done for all

capillaries. If the mean intensity at each run is within one standard deviation of the other runs, then this source of variation is considered insignificant.

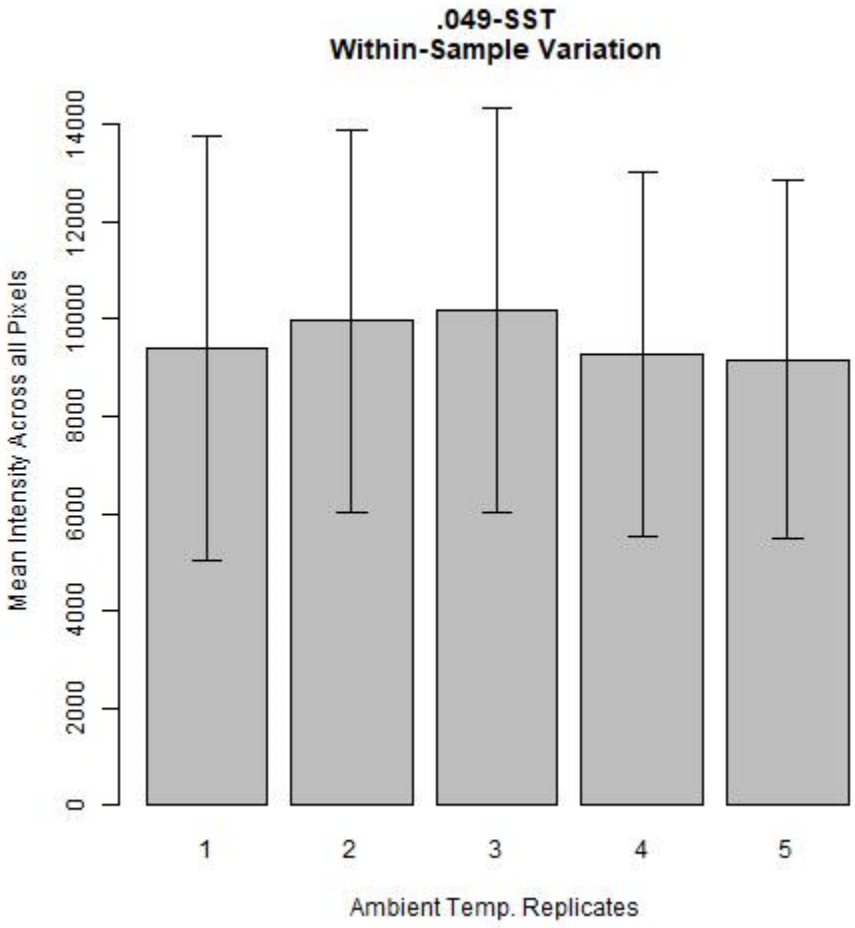

Figure 37: Within- sample variation is displayed as a bar plot of mean intensity within the 880-890 m/z range that each pixel experiences for the ambient experiment. The standard deviation of mean intensity among the pixels is included as an error bar. In this figure, the mean intensity for all five ambient replicates falls comfortably within one standard deviation of each other.

Additional processing for each capillary includes plotting mass spectra within the 880- 890 mass range and the mean intensity as a function of temperature to understand how the geometry is affecting heating efficiency, as well as signal intensity.

7.2.4 Between Capillary Analysis

Between capillary analysis involves comparing the total intensity of ions collected by the capillaries within the 880- 890 mass range. Capillaries are analyzed based on the two parameters: inner diameter and cross-sectional profile. .039”-SST, the smallest circular cross-section capillary, is used as a comparison of a standard capillary to the different cross-sectional profiles. The goal here is to identify how well a capillary is increasing signal intensity as temperature increases, compared to other capillaries. Simply put, changes in sensitivity to heating due to geometry are evaluated.

CHAPTER 8

RESULTS AND DISCUSSION

8.1 Verifying the Effect of Temperature on Intensity

The effect of temperature on intensity can be summarized from the results of the experiments for each capillary. All seven of the capillaries that are tested showed an increase in total intensity as they were heated. The relative intensity increase in the mass spectrum in the 880-890 *m/z* is shown for the web-type capillary in Figure 38. The relative intensity is the sum of all the mass spectra for all pixels in a replicate normalized to the ambient replicates. For this capillary, there is a five times increase in the peak signal at 885 *m/z* from ambient to 100˚C. There is another jump from 100˚C to 200˚C, and a final jump from 200˚C to 300˚C, with the intensity at 300˚C over 30 times that of ambient. This plot, as well as the rest of the relative intensity plots (not included), validates the positive effect of increasing temperature on signal intensity. The rate at which signal intensity increases with respect to temperature is still dependent on capillary geometry, discussed in the next few sections.

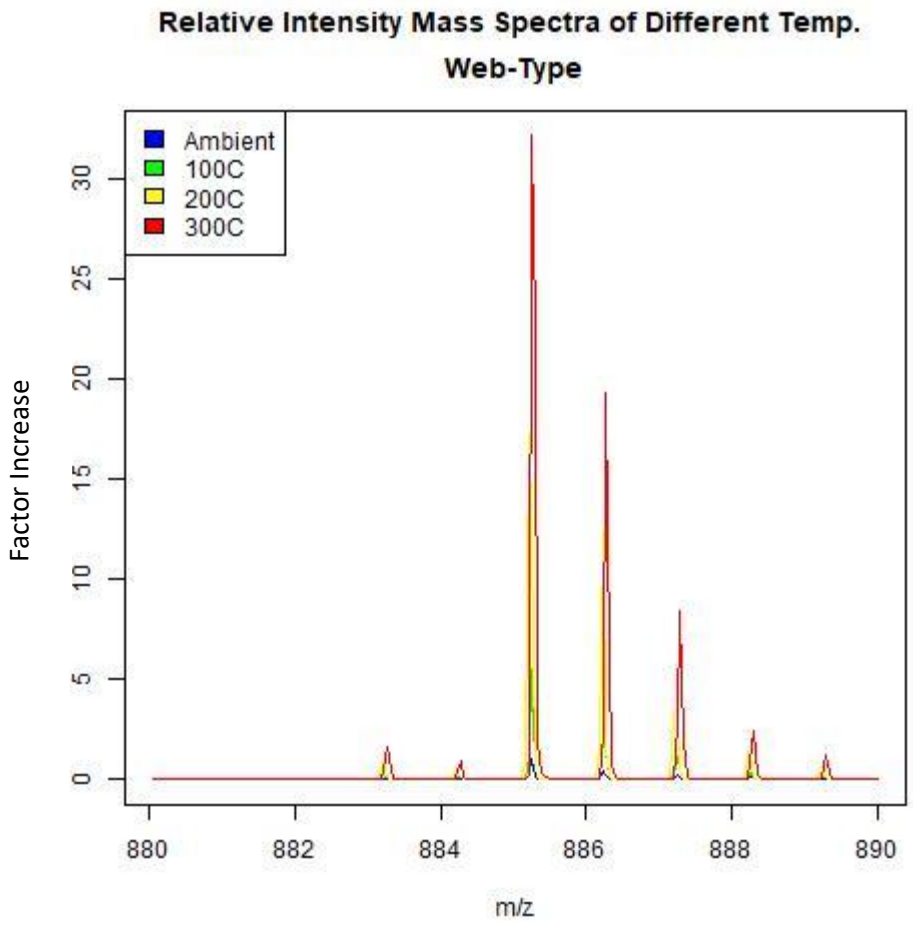

Figure 38: Relative intensity mass spectra at different temperatures for the web-type capillary. The primary peak occurs at 885 m/z, which corresponds with the prior knowledge of pig liver composition. The three cascading peaks immediately after 885 are isotopes.

8.2 Cross-Sectional Profile

8.2.1 Results

Intensity as a function of temperature is shown for all capillary cross-section types (Figure 39). Out of the five cross-sections, the circular .039”-SST capillary has the highest overall signal intensity at 300˚C. Dual-channel does perform slightly better than .039”-SST at 100˚C and 200˚C but drops off at 300˚C. This could potentially be due to some change in ambient condition, or some sample variation, as the dual-channel control experiments for 300˚C show a decrease in intensity

from the previous temperatures (Figure 40). All other capillaries had no significant within-sample and sample-to-sample variation. This helps ensure that variation is not the primary cause for the results that are acquired; instead, they should be primarily based on the capillary geometry.

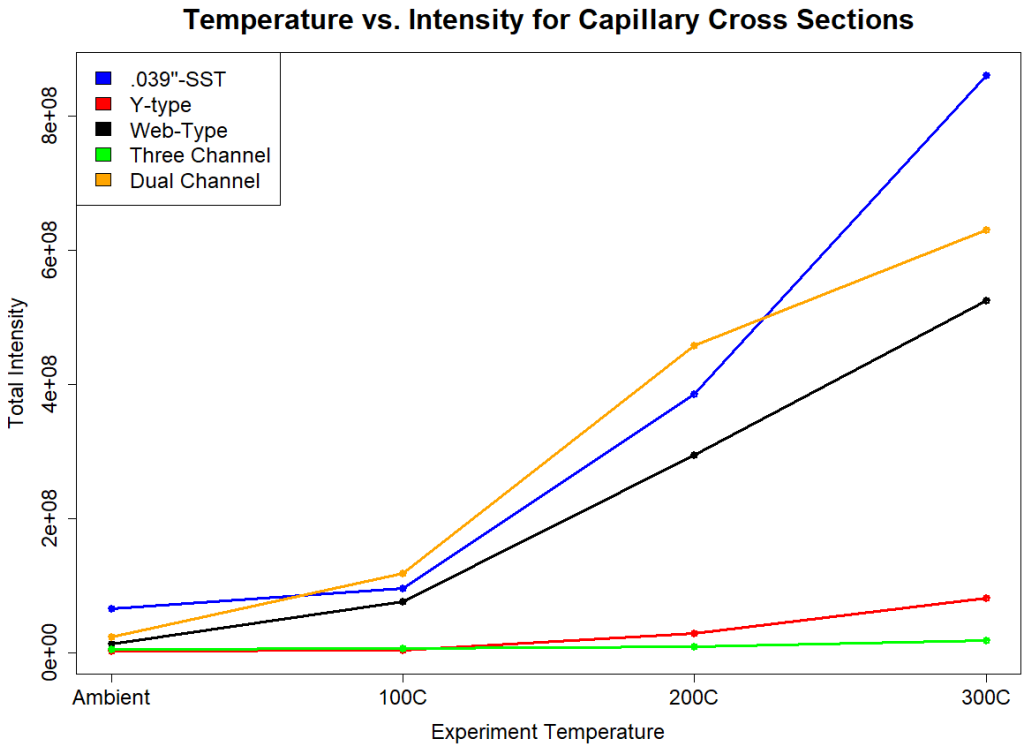

Figure 39: Total Intensity vs. Temperature for different capillary cross sections

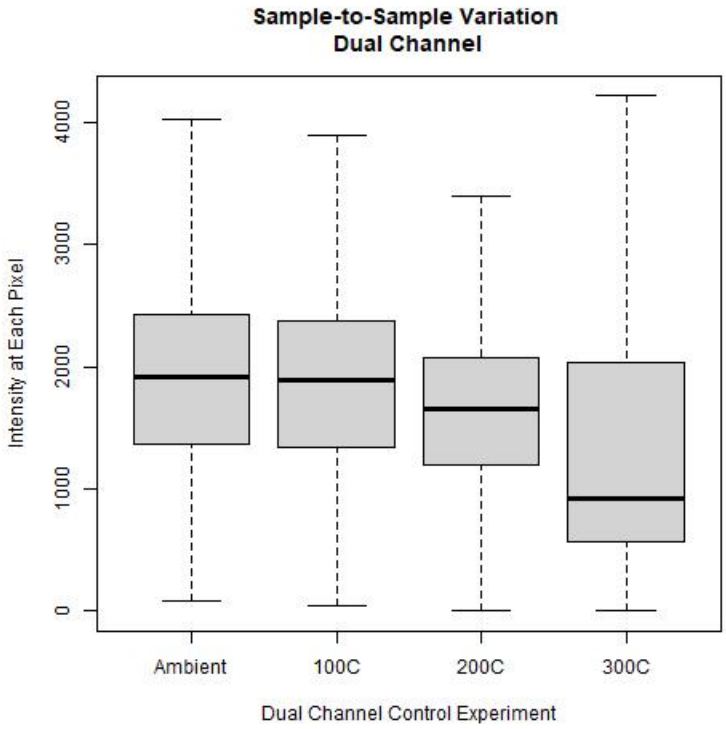

Figure 40: Dual channel control experiments at every temperature. The control-start and control-end experiment at 300˚C is slightly lower than the other temperatures, indicating some negative sample variation

The y-type and three-channel cross-sections perform poorly at every temperature, compared to the other cross-sections. These two capillaries have the smallest flow area. The small flow area could potentially inhibit the capture of entrenched ions, decreasing overall intensity. At ambient temperature, the signal intensity for all non-circular cross-sections is lower than that of the circular cross-section (Figure 41). Out of the non-circular cross-sections, dual-channel and the web type perform better at ambient conditions. Dual-channel, which has the highest flow area out of the four non-circular cross-sections, performs the best at ambient. Web type, which has the second-highest flow area, performs the second-best at ambient, indicating a positive relationship between flow area and signal intensity.

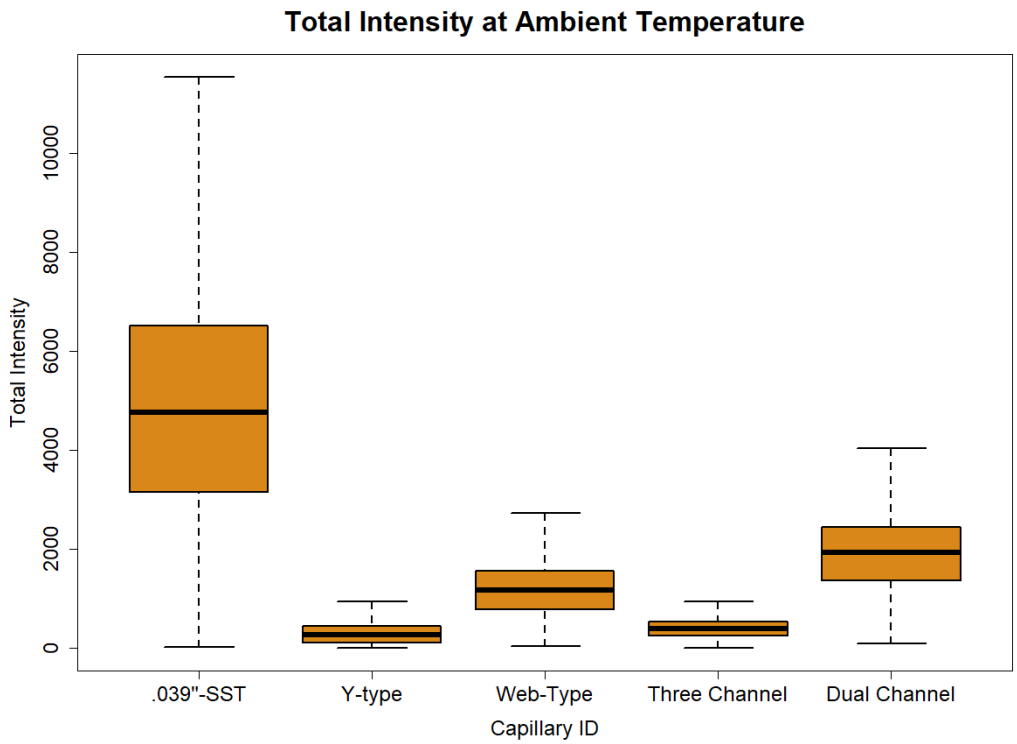

Figure 41: Total intensity at each pixel at ambient temperature for all cross-sections. The circular cross-section .039"-SST is providing a higher signal intensity at ambient temperature compared to the other cross-sections.

Although .039"-SST has the highest total signal intensity, the dual-channel, web-type, and y-type cross-sections all have a steeper increase in signal intensity as temperature increases (Figure 42). Dual-channel and web-type are the more interesting of the three, as they had comparable total intensities to the .039"-SST. Web type has the highest factor increase from ambient to 300˚C, at approximately 40x signal intensity. This is almost 4x greater than that of .039"-SST, indicating that the capillary geometry, such as max particle distance, did play a role in increasing sensitivity of the ion flow to heating. The dual-channel curve follows the web-type curve closely, but drops off at 300˚C, potentially due to sample variation mentioned previously.

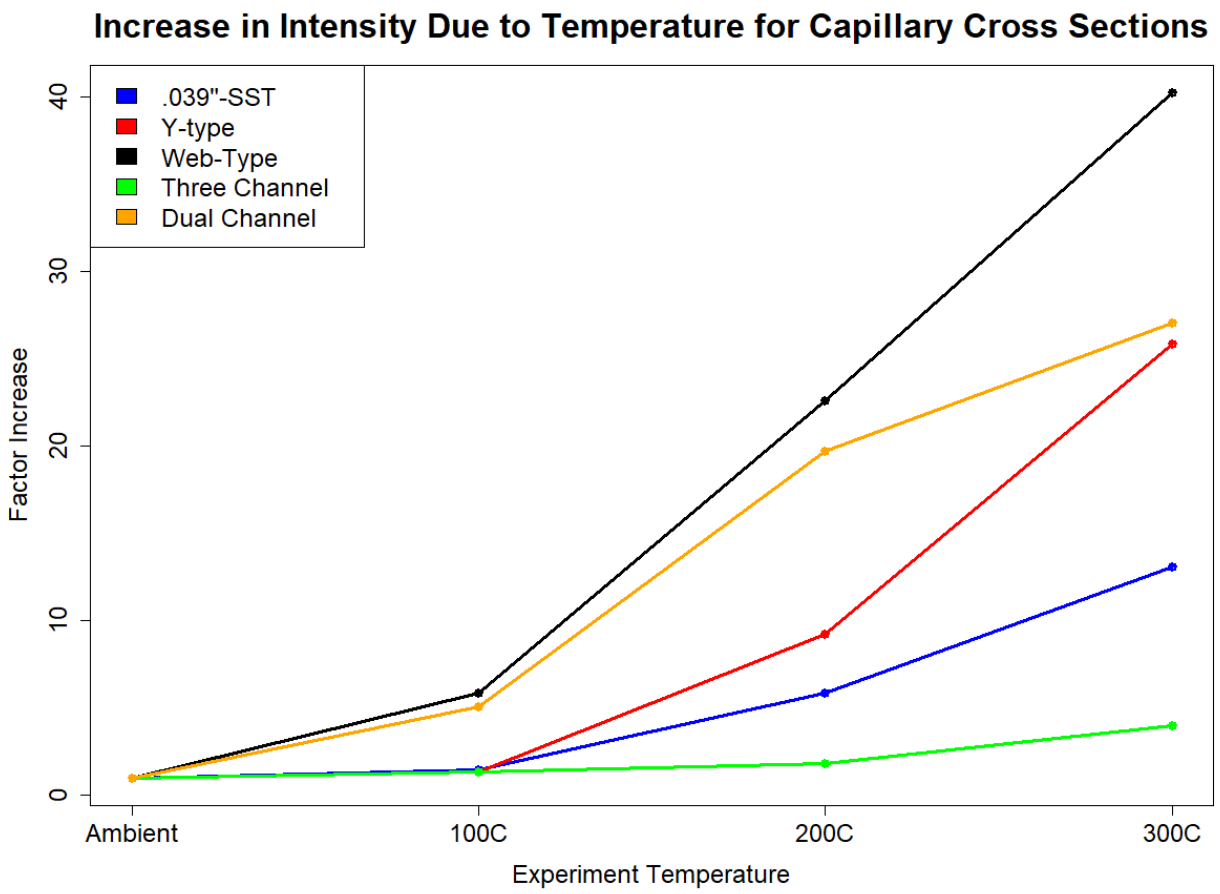

Figure 42: Increase in intensity due to temperature for capillary cross-sections. This plot is created by normalizing each cross-section's elevated temperature replicate intensity with its own ambient intensity data. The web-type has the steepest increase in intensity as temperature increases, followed by dual-channel, and then y-type.

8.3 Cross-Section Performance Inhibitors

Two potential inhibitors may have had an impact on the performance of the brass capillaries. The first is the flow restrictor cone and its placement in relation to the capillary potentially inhibiting flow rate. The sagging of the brass capillaries at elevated temperature is the second issue.

8.3.1 Inhibitor #1: Flow Restrictor

The flow restrictor is inserted into the nose cone and has two purposes. First, it has an O-ring seal that prevents the ambient pressure from leaking into the MS system. Second, there is an orifice on the end that is closest to the capillary that has a small ID. This is to ensure the MS does not experience too high of flow from the capillary opening. The issue here is that the restrictor orifice is centered on the inner channel walls for the non-standard cross-sections (Figure 43). This plays a significant role in limiting the flow area from the outlet end and thus affect MS signal intensity.

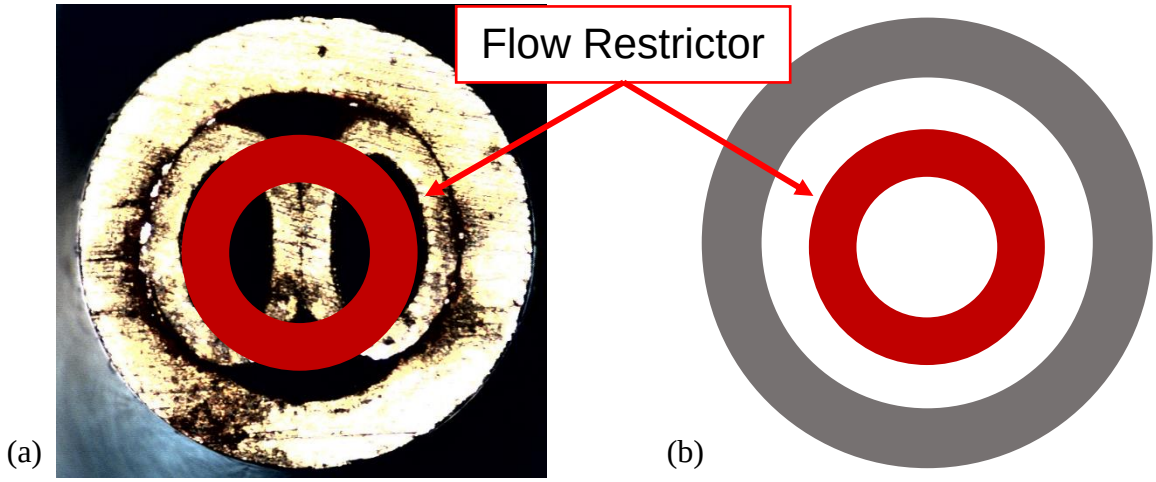

Figure 43: Flow restrictor interaction with a non-standard vs. circular cross-section. (a) The flow restrictor lines up with the walls of the inner channels, impeding flow into the MS. (b) The flow restrictor does not impede any flow in a circular cross-section tube as there is no center wall.

Flow rate measurements are taken to gain a better understanding of how the flow restrictor and flow area affect the flow rate within the capillary. An ALICAT flow meter is used to capture flow rate information (Figure 44).

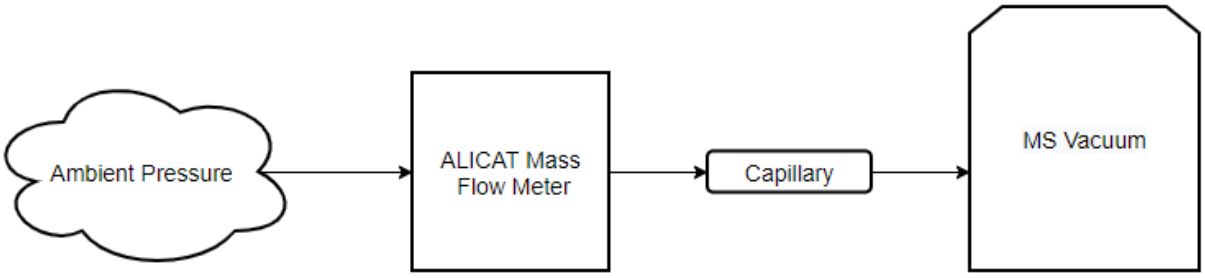

Figure 44: Diagram of flow rate measurement setup

Data indicates that the non-circular cross-sections are seeing reduced flow, due to either the flow restrictor, the reduced flow area, or both (Table 5). The circular cross-sections have their flow rate level off after the .039”-SST, indicating that the flow restrictor is indeed choking flow after a specific ID. A plot of the volumetric flow rate vs. flow area for the brass capillaries shows a non-linear relationship, indicating that the flow restrictor is likely playing a role in limiting flow rate (Figure 45).

Table 5: Volumetric Flow Rate Data

Type	Flow Rate (SLPM)	Flow Area (m^2)	Inlet Velocity (m/s)
0.063"-SST	2.88	2.01E-06	23.9
0.049"-SST	2.845	1.22E-06	39.0
0.039"-SST	2.688	7.71E-07	58.1
Y-Type	1.286	5.34E-07	40.2
Web -Type	1.802	5.82E-07	51.6
Dual Channel	1.904	7.81E-07	40.7
Three Channel	0.862	5.34E-07	26.9

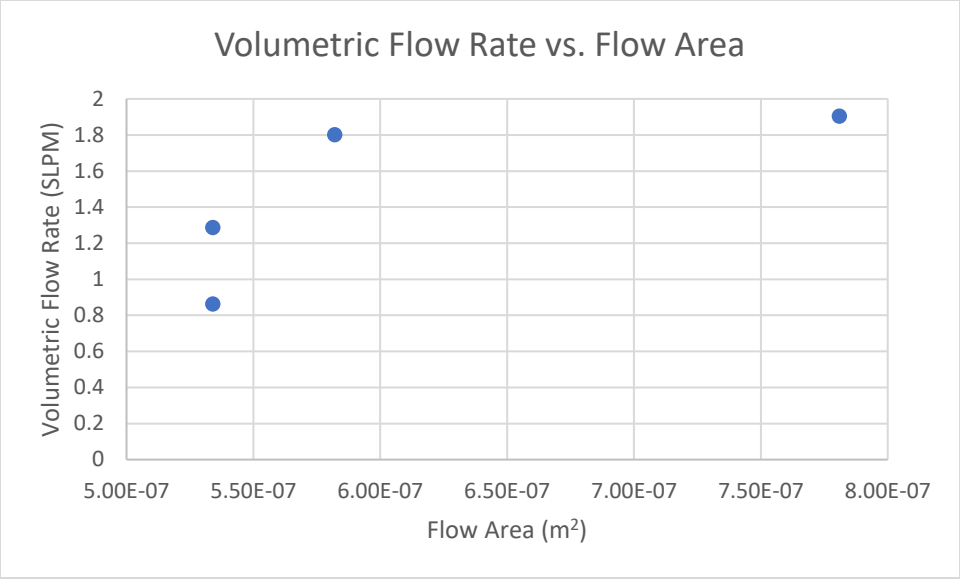

Figure 45: Volumetric Flow Rate vs. Flow Area for non-circular cross-section capillaries. A linear relationship does not seem to exist

8.3.2 Inhibitor #2: Brass Capillary Sagging at Elevated Temperatures

The second inhibitor stems from the material properties of brass. As previously discussed, brass has a low melting point compared to SST. When elevated to even 300˚C, the capillary begins to sag (Figure 46). During experiments, the capillary has sagged to point it has touched the sample stage. Positional accuracy is vital to keeping up the signal intensity; sagging disrupts capillary position. Although the position was reset between replicates, capillaries still sagged throughout the replicate run. This may have inhibited the brass capillaries from having an even greater increase in signal intensity at 300˚C than recorded.

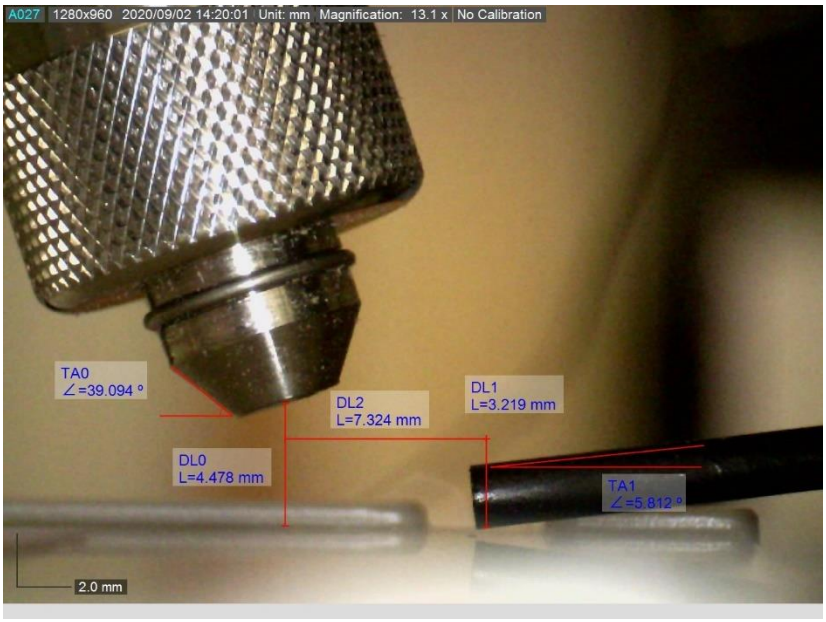

Figure 46: Brass capillary sagging from the drawn optimal position

8.4 Inner Diameter

Out of the three capillaries used for testing the ID parameter, the .049”-SST capillary performed the best at elevated temperatures (Figure 47). The capillary improves performance at every temperature, seeing a sharp jump in intensity from 200˚C to 300˚C. There is potential for an additional jump in intensity at even higher temperatures, as the relationship appears to be exponential.

The .039”-SST has the lowest total signal intensities overall, about a magnitude smaller than the .049”-SST at 300˚C. This can be attributed to a smaller flow area, as well as a lower volumetric flow rate. As seen with the brass capillaries, the flow area and volumetric flow rate do affect signal intensity.

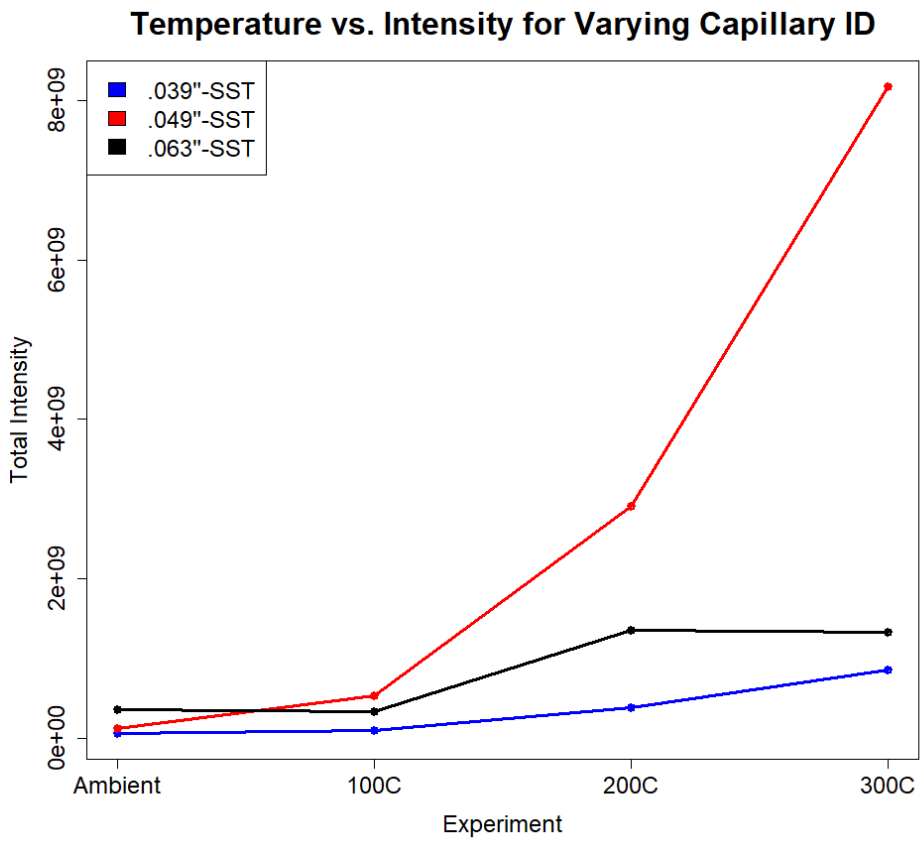

Figure 47: Temperature vs. intensity for different capillary ID. The .049”-SST has the highest overall intensity at 300˚C.

The total intensity curve for the .063”-SST capillary increases from 100˚C to 200˚C then levels off at 300˚C. This supports the hypothesis that a capillary with a larger ID would have lower signal intensities at elevated temperatures due to decreased heating at the center of the flow. However, the control experiments for the .063”-SST indicate that there is some variation within the sample or ambient conditions that affected the 300˚C replicates (Figure 48).

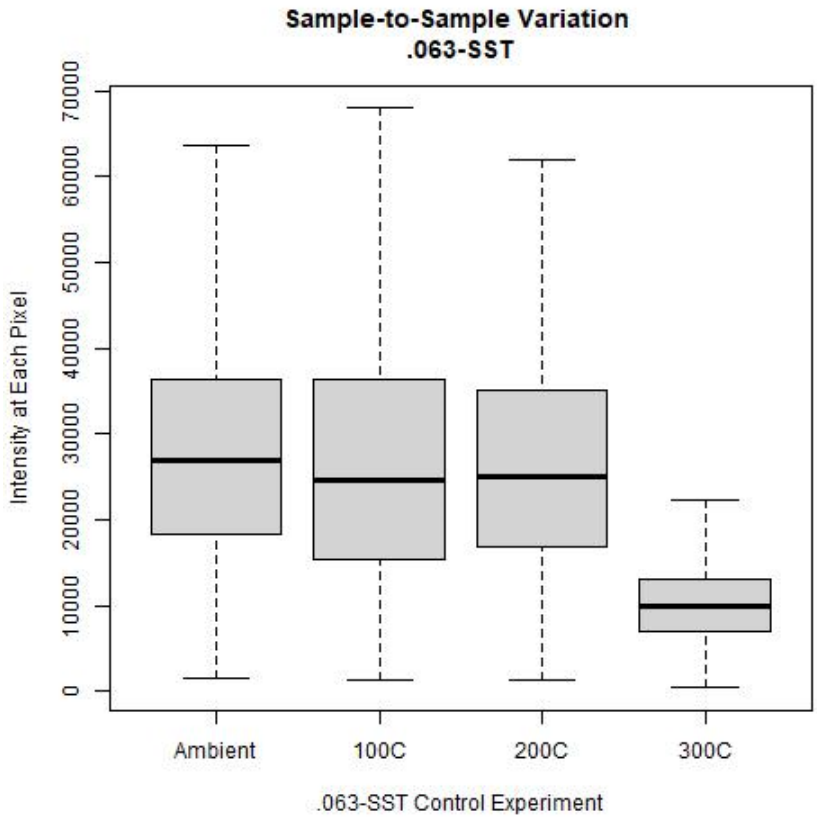

Figure 48: Sample-to-sample variation of .063"-SST capillary. The 300˚C control experiments are lower than the others, indicating some negative variation for this set of experiments.

At ambient temperature, the signal intensity scales from smallest to largest ID (Figure 49). The larger ID indicates a larger flow area; the larger flow area can capture a larger quantity of the entrenched ions. It is important to note that the .049”-SST and .063”-SST have the same volumetric flow rate. The flow restrictor caps their flow rate at 2.888 SLPM, as seen in Table 5. This indicates that the increase in intensity due to ID at ambient temperature is due to the larger flow area, not because of an increase in volumetric flow rate.

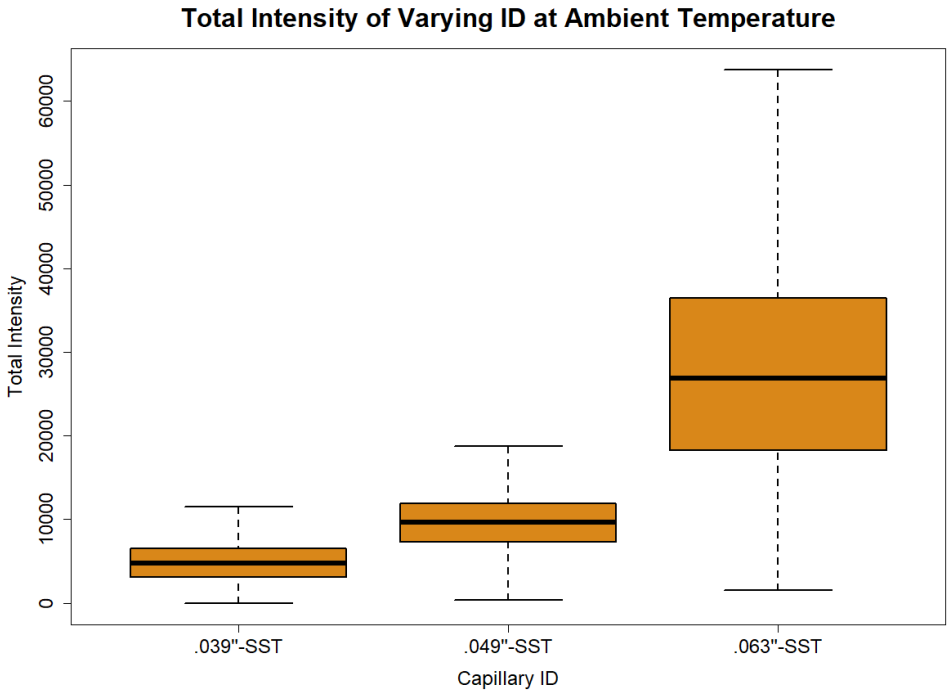

Figure 49: Total intensity for each pixel for different capillary ID at ambient temperature.

In addition to the highest overall intensity, the .049”-SST also had the greatest factor increase from ambient to 300˚C, with approximately a 70x increase in intensity (Figure 50). The .063”-SST does have the worst heating sensitivity as the largest capillary. The .039”-SST only performs slightly better. This does not support the hypothesis that a smaller ID capillary will improve signal intensity due to increased ion desolvation. It cannot exactly be determined if desolvation is better in the .039”-SST or .049”-SST, as the signal intensity can be lower in the former capillary even if the transmission efficiency is higher due to increased desolvation. However, the conclusion can be made that there is an optimal ID for signal intensity and heating sensitivity. Too small of an ID may not capture enough of the ion flow, decreasing flow rate even with a reduced flow area. The decreased flow rate may lead to higher ion residence times, and thus, higher ion losses to the wall. On the other hand, too large of an ID will not provide high sensitivity to heating.

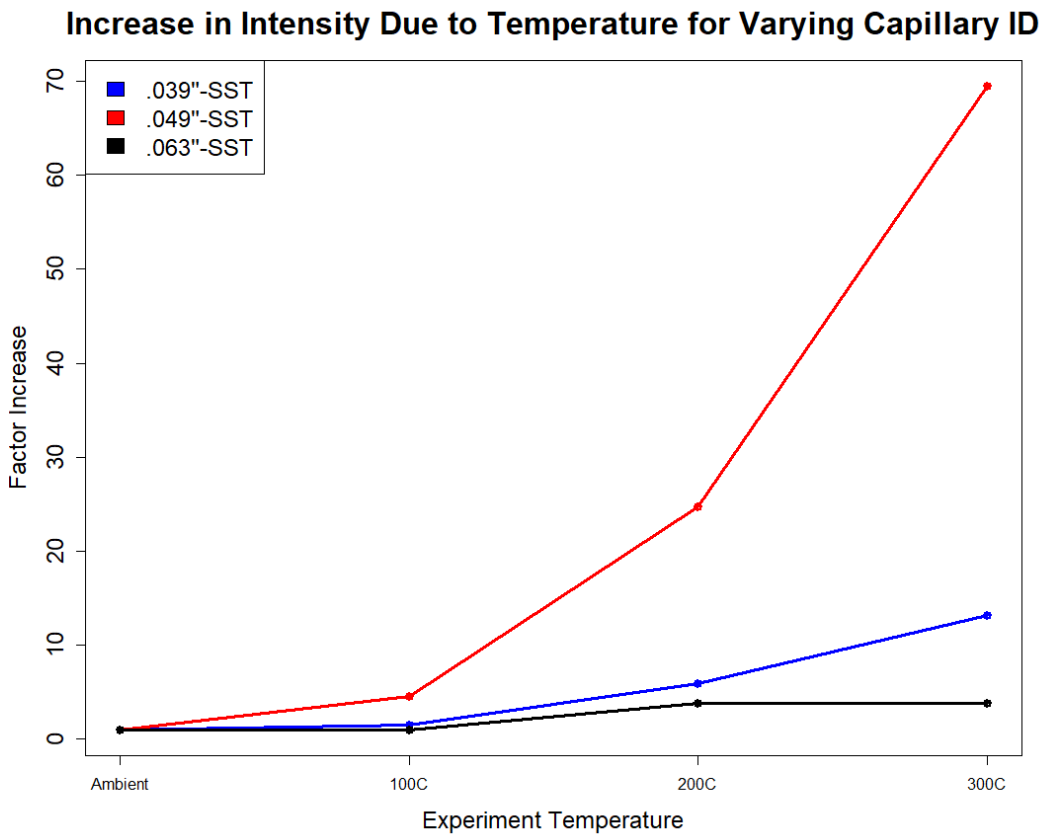

Figure 50: Increase in intensity due to temperature for different capillary ID

CHAPTER 9

CONCLUSIONS AND FUTURE WORK

The experiments surrounding the two selected parameters provide insight into how different factors interplay to affect the signal intensity of the MS. The hypothesis that a decreased particle distance may provide increased signal intensity due to increased ion desolvation appears to be true in the case of the non-circular cross-sections. When compared with a circular cross-section of similar flow area, the web-type and dual-channel cross-sections clearly provide increased ion desolvation, as evidenced by the increase in sensitivity to heating. However, this is not the case for the y-type and three-channel cross-sections, possibly due to the much lower flow area and volumetric flow rate.

Regarding the circular capillaries, there appears to be an optimal ID. A capillary that is too small may not capture enough sample to have heating sensitivity make an impact. A capillary that is too large will not benefit from heating due to the decreased temperature boundary layer thickness. The current Waters capillary with a .049" ID appears to be the optimal size for both ion capture and sensitivity to heat.

There is significant potential for future work with non-circular capillary cross-sections. Some of the data collected in this experiment may be lower due to a smaller flow area and a slower volumetric flow rate. Testing these cross-sections, especially the web-type and dual-channel, at a larger capillary size may provide a better combination of heating sensitivity and flow rate to increase overall signal intensity. Eliminating the inhibitors such as the flow restrictor and sagging can also help improve results. Design changes to the flow restrictor and capillary interface can be

made to increase the flow rate. Producing these cross-sections in a material with a higher melting point, such as SST, can alleviate sagging. Using a material such as SST also allows for testing at higher temperatures.

Hsu continues this project at Waters Corporation. The results in this thesis will be used to shape the experiments for non-circular capillaries that are larger and more comparable in flow area to the .049”-SST. Flow simulation for each of the capillaries is also in progress and is key to understanding the heating at the center of the flow. The results from all these experiments can be used by Waters to provide clients with a capillary-heater design that improves both the usability and effectiveness of the MS system.

APPENDIX

R SCRIPT

Listing A-1: Within- Capillary Processing

```
## Imports
library(Cardinal)
library(rem)
library(data.table)

# Read .iMZML files for specifc experiment type
exp_type <- ".049-SST"
file_type <- "049SST"

path_in_all <- paste0(c(rep(file_type)),
                      c("_Ambient_ControlStart on DESI MS_1",
                        "_Ambient_Replicate1 on DESI MS_1",
                        "_Ambient_Replicate2 on DESI MS_1",
                        "_Ambient_Replicate3 on DESI MS_1",
                        "_Ambient_ControlEnd on DESI MS_1",
                        "_100C_ControlStart on DESI MS_1",
                        "_100C_Replicate1 on DESI MS_1",
                        "_100C_Replicate2 on DESI MS_1",
                        "_100C_Replicate3 on DESI MS_1",
                        "_100C_ControlEnd on DESI MS_1",
                        "_200C_ControlStart on DESI MS_1",
                        "_200C_Replicate1 on DESI MS_1",
                        "_200C_Replicate2 on DESI MS_1",
                        "_200C_Replicate3 on DESI MS_1",
                        "_200C_ControlEnd on DESI MS_1",
                        "_300C_ControlStart on DESI MS_1",
                        "_300C_Replicate1 on DESI MS_1",
                        "_300C_Replicate2 on DESI MS_1",
                        "_300C_Replicate3 on DESI MS_1",
                        "_300C_ControlEnd on DESI MS_1"), c(rep(".imzml",20)))

msi_all <- vector(mode="list", length = 20) # Initialize list of MassImagingExperiments

## Read all data for given cross-section and temp.
## resolution =  and units = "ppm" for updating bin size
## mass.range = c(x1,x2) to specify mass range
for(i in 1:length(path_in_all)) {
  cat("\n", path_in_all[i], "\n")
  msi_all[i] <- readMSIData(path_in_all[i], resolution = 50, attach.only=TRUE)
}

## Print info regarding Data
for(i in 1:length(msi_all)) {
  cat("\n", path_in_all[i], "\n")
  print(imageData(msi_all[[i]]))
}

## Statistics
temp_arr <- paste0(c("Ambient","100C", "200C", "300C"))
msi_subset <- vector(mode="list", length = 20) # Initialize list of MassImagingExperiments
tic_sub <- array(dim = length(1))
mean_sub <- array(dim = length(1))
sd_sub <- array(dim = length(1))
```

```
for(i in 1:length(msi_all)) {
  cat("\n", path_in_all[i], "\n")

  msi_subset[i] <- subsetFeatures(msi_all[[i]], mz > 880, mz < 890)
  tic_sub[i] <- sum(pixelApply(msi_subset[[i]], sum)) # Sum of ion count in m/z range across each pixel
  mean_sub[i] <- mean(pixelApply(msi_subset[[i]], sum)) # Mean total intensity across all pixels of an experiment
  sd_sub[i] <- sd(pixelApply(msi_subset[[i]], sum)) # Std. Dev. of total intensity across all pixels of an experiment
}

## Intensity Mass Spectra 880 - 890 m/z

ambient <- (featureApply(msi_subset[[2]], sum))
hundred <- (featureApply(msi_subset[[7]], sum))
two <- (featureApply(msi_subset[[12]], sum))
three <- (featureApply(msi_subset[[17]], sum))
mass_range <- mz(msi_subset[[1]])

## Individual Plot
jpeg(file=paste0(c("C:/Users/asus/Documents/DESI_Data/All_iMZML/Plots/880-890_Ambient"), exp_type, c(".png")))
plot(mass_range,ambient, type = "l", col = "blue",
    main = paste0(c("Mass Spectrum \n", exp_type,
                switch(1, "Ambient", "100C", "200C", "300C"))),
    xlab = "m/z", ylab = "Intensity")
dev.off()

jpeg(file=paste0(c("C:/Users/asus/Documents/DESI_Data/All_iMZML/Plots/880-890_100C"), exp_type, c(".png")))
plot(mass_range, hundred, type = "l", col = "blue",
    main = paste0(c("Mass Spectrum \n", exp_type,
                switch(2, "Ambient", "100C", "200C", "300C"))),
    xlab = "m/z", ylab = "Intensity")
dev.off()

jpeg(file=paste0(c("C:/Users/asus/Documents/DESI_Data/All_iMZML/Plots/880-890_200C"), exp_type, c(".png")))
plot(mass_range, two, type = "l", col = "blue",
    main = paste0(c("Mass Spectrum \n", exp_type,
                switch(3, "Ambient", "100C", "200C", "300C"))),
    xlab = "m/z", ylab = "Intensity")
dev.off()

jpeg(file=paste0(c("C:/Users/asus/Documents/DESI_Data/All_iMZML/Plots/880-890_300C"), exp_type, c(".png")))
plot(mass_range, three, type = "l", col = "blue",
    main = paste0(c("Mass Spectrum \n", exp_type,
                switch(4, "Ambient", "100C", "200C", "300C"))),
    xlab = "m/z", ylab = "Intensity")
dev.off()

## Superimposed
ylim_max = max(c(ambient, hundred, two, three))

jpeg(file=paste0(c("C:/Users/asus/Documents/DESI_Data/All_iMZML/Plots/880-890_All"), exp_type, c(".png")))
plot(mass_range,ambient, type = "l", col = "blue",
    main = paste0(c("Mass Spectra of Different Temp. \n", exp_type)),
    xlab = "m/z", ylab = "Intensity", ylim = c(0, ylim_max))
lines(mass_range,hundred,col="green")
lines(mass_range,two,col="yellow")
lines(mass_range,three,col="red")
legend("topleft", legend=(temp_arr), fill = c("blue", "green", "yellow", "red"))
dev.off()


## Relative Intensity Mass Spectra M/Z 880- 890
ambient_norm <- ambient / max(ambient)
hundred_norm <- hundred / max(ambient)
two_norm <- two / max(ambient)
three_norm <- three / max(ambient)

jpeg(file=paste0(c("C:/Users/asus/Documents/DESI_Data/All_iMZML/Plots/880_890_Relative"), exp_type, c(".png")))
ylim_max = max(c(ambient_norm, hundred_norm, two_norm, three_norm))
```

```
plot(mass_range,ambient_norm, type = "l", col = "blue",
    main = paste0(c("Relative Intensity Mass Spectra of Different Temp. \n", exp_type)),
    xlab = "m/z", ylab = "Intensity", ylim = c(0, ylim_max))
lines(mass_range,hundred_norm,col="green")
lines(mass_range,two_norm,col="yellow")
lines(mass_range,three_norm,col="red")
legend("topleft", legend=(temp_arr), fill = c("blue", "green", "yellow", "red"))
dev.off()

## Relative Intensity for 50- 1200 m/z
ambient_all <- (featureApply(msi_all[[2]], sum))
hundred_all <- (featureApply(msi_all[[7]], sum))
two_all <- (featureApply(msi_all[[12]], sum))
three_all <- (featureApply(msi_all[[17]], sum))
mass_range <- mz(msi_all[[1]])


## Superimposed
ylim_max = max(c(ambient, hundred, two, three))

jpeg(file=paste0(c("C:/Users/asus/Documents/DESI_Data/All_iMZML/Plots/all_All"), exp_type, c(".png")))
plot(mass_range,ambient_all, type = "l", col = "blue",
    main = paste0(c("Mass Spectra of Different Temp. \n", exp_type)),
    xlab = "m/z", ylab = "Intensity", ylim = c(0, ylim_max+1.25*ylim_max))
lines(mass_range1,hundred_all,col="green")
lines(mass_range2,two_all,col="yellow")
lines(mass_range3,three_all,col="red")
legend("topleft", legend=(temp_arr), fill = c("blue", "green", "yellow", "red"))
dev.off()

## Standard Deviation of Intensity Across Pixels
sd_pooled <- c(sqrt(sum(sd_sub[2:4]^2/3)),
               sqrt(sum(sd_sub[7:9]^2/3)),
               sqrt(sum(sd_sub[12:14]^2/3)),
               sqrt(sum(sd_sub[17:19]^2/3)))

sd_mat <- c(sd_sub[2:4], sd_sub[7:9], sd_sub[12:14], sd_sub[17:19])

saveRDS(sd_pooled, file = paste0(file_type, c("_sd_pooled.RDS")))
saveRDS(sd_mat, file = paste0(file_type, c("_sd_mat.RDS")))

jpeg(file=paste0(c("C:/Users/asus/Documents/DESI_Data/All_iMZML/Plots/Std_Intensity_Across"), exp_type, c(".png")))
plot(sd_pooled, type="o", col = "blue",
    main = paste0(c("Standard Deviation of Intensity Across Pixels", exp_type)),
    xlab = "Experiment", ylab = "Intensity", xaxt = "n")
axis(1, at = 1:4, labels = temp_arr)
dev.off()

## Total Ion Current Across Pixels for Replicates of Each Temp.
tic_sum <- c((sum(tic_sub[2:4])),
             (sum(tic_sub[7:9])),
             (sum(tic_sub[12:14])),
             (sum(tic_sub[17:19])))

tic_sum_mat <- c(((tic_sub[2:4])),
                 ((tic_sub[7:9])),
                 ((tic_sub[12:14])),
                 ((tic_sub[17:19])))

saveRDS(tic_sum, file = paste0(file_type, c("_tic_sum.RDS")))
saveRDS(tic_sum_mat, file = paste0(file_type, c("_tic_sum_mat.RDS")))


jpeg(file=paste0(c("C:/Users/asus/Documents/DESI_Data/All_iMZML/Plots/Total_Intensity_"), exp_type, c(".png")))
plot(tic_sum, type="o", col = "blue",
    main = paste0(c("Total Intensity Across Pixels\n"), exp_type),
    xlab = "Experiment", ylab = "Intensity", xaxt = "n")
axis(1, at = 1:4, labels = temp_arr)
```

```
dev.off()

jpeg(file=paste0(c("C:/Users/asus/Documents/DESI_Data/All_iMZML/Plots/Total_Intensity_Relative"), exp_type, c(".png")))
plot(tic_sum / tic_sum[1], type="o", col = "blue",
    main = paste0(c("Intensity vs Temp. Across Pixels\n"), exp_type),
    xlab = "Experiment", ylab = "Factor Increase", xaxt = "n")
axis(1, at = 1:4, labels = temp_arr)
dev.off()

# Mean Current Across Pixels
tic_mean <- c((mean(mean_sub[2:4])),
              (mean(mean_sub[7:9])),
              (mean(mean_sub[12:14])),
              (mean(mean_sub[17:19])))

tic_mean_mat <- c(((mean_sub[2:4])),
                  ((mean_sub[7:9])),
                  ((mean_sub[12:14])),
                  ((mean_sub[17:19])))

saveRDS(tic_mean, file = paste0(file_type, c("_tic_mean.RDS")))
saveRDS(tic_mean_mat, file = paste0(file_type, c("_tic_mean_mat.RDS")))

jpeg(file=paste0(c("C:/Users/asus/Documents/DESI_Data/All_iMZML/Plots/Mean_Intensity"), exp_type, c(".png")))
mean_plot <- plot(tic_mean, type="o", col = "blue",
                  main = paste0(c("Mean Intensity Across Pixels", exp_type)),
                  xlab = "Experiment", ylab = "Intensity", xaxt = "n",
                  ylim = c(0,max(tic_mean + sd_pooled)))
axis(1, at = 1:4, labels = temp_arr)

segments(x0 = 1:4, y0 = tic_mean - sd_pooled, x1 = 1:4,
         y1 = tic_mean + sd_pooled, lwd = 1.5)
arrows(x0 = 1:4, y0 = tic_mean - sd_pooled, x1 = 1:4,
       y1 = tic_mean + sd_pooled, lwd = 1.5, angle = 90,
       code = 3, length = .1)
dev.off()


## Sample to Sample Variation
control_var <- (c((pixelApply(msi_subset[[1]], sum)),
                  (pixelApply(msi_subset[[2]], sum)),
                  (pixelApply(msi_subset[[3]], sum)),
                  (pixelApply(msi_subset[[4]], sum)),
                  (pixelApply(msi_subset[[5]], sum))))

t100_var <- (c((pixelApply(msi_subset[[6]], sum)),
               (pixelApply(msi_subset[[10]], sum))))

t200_var <- (c((pixelApply(msi_subset[[11]], sum)),
               (pixelApply(msi_subset[[15]], sum))))

t300_var <- (c((pixelApply(msi_subset[[16]], sum)),
               (pixelApply(msi_subset[[20]], sum))))

saveRDS(control_var, file = paste0(file_type, c("_control_var.RDS")))
saveRDS(t100_var, file = paste0(file_type, c("_t100_var.RDS")))
saveRDS(t200_var, file = paste0(file_type, c("_t200_var.RDS")))
saveRDS(t300_var, file = paste0(file_type, c("_t300_var.RDS")))

jpeg(file=paste0(c("C:/Users/asus/Documents/DESI_Data/All_iMZML/Plots/Control_Variation_"), exp_type, c(".png")))
boxplot(control_var, t100_var, t200_var, t300_var, xaxt = "n", main =
          paste0(c("Sample-to-Sample Variation \n"), exp_type),
        xlab = paste(exp_type, "Control Experiment"),
        ylab = "Intensity at Each Pixel", outline = FALSE)
axis(1, at = 1:4, labels = temp_arr)
dev.off()

## Within Sample Variation
```

```
## Average TIC seen by each pixel for all control experiment
control_var_mean <- (c(mean_sub[1], mean_sub[2], mean_sub[3], mean_sub[4], mean_sub[5]))

## Standard Deviations of TIC seen by each pixel for all control experiment
control_var_sd <- (c(sd_sub[1], sd_sub[2], sd_sub[3], sd_sub[4], sd_sub[5]))

control_mean <- mean(control_var_mean)

control_sd <- sqrt(sum((control_var_sd^2)/5)) ##Combine St. Dev to find Population Standard Deviation

jpeg(file=paste0(c("C:/Users/asus/Documents/DESI_Data/All_iMZML/Plots/Within_Sample_Variation_"), exp_type, c(".png")))
par(mar=c(4,4,2,1) + 1)
bart <- barplot(control_var_mean,
                main = paste0(c(exp_type, "Within-Sample Variation")),
                width = 10,
                names.arg = c(1:5),
                xlab = "Ambient Temp. Replicates", ylab = "Mean Intensity Across all Pixels",
                ylim = range(pretty(c(0, control_var_mean + control_var_sd))))
segments(bart, y0 = control_var_mean - control_var_sd, bart,
         y1 = control_var_mean + control_var_sd, lwd = 1.5)
arrows(bart, y0 = control_var_mean - control_var_sd, bart,
       y1 = control_var_mean + control_var_sd, lwd = 1.5, angle = 90,
       code = 3, length = .1)
dev.off()
```

Listing A2: Between Capillary Processing

```
## Imports
library(Cardinal)
library(rem)
library(data.table)

temp_arr <- paste0(c("Ambient","100C", "200C", "300C"))
rep_arr <- c("Rep. 1", "Rep. 2", "Rep. 3")
# Recall Capillary Information From Memory
exp_type <- c(".039\"-SST", "Y-type", "Web-Type", "Three Channel", "Dual Channel")
file_type <- c("039SST", "YType", "Web", "Three", "Dual")

# Initialize arrays to store data from memory
tic_sums <- array()
tic_means <- array()
tic_mean_mats <- array()
tic_sum_mats <- array()
control_vars <- array()
t100_vars <- array()
t200_vars <- array()
t300_vars <- array()

# Recall data for each capillary type
for(i in 1:(length(file_type))) {
  if(i == 1) {
    tic_sums <- (readRDS(paste0(file_type[i], c("_tic_sum.RDS"))))
    t100_vars <- (readRDS(paste0(file_type[i], c("_t100_var.RDS"))))
    t200_vars <- (readRDS(paste0(file_type[i], c("_t200_var.RDS"))))
    t300_vars <- (readRDS(paste0(file_type[i], c("_t300_var.RDS"))))
    control_vars <- (readRDS(paste0(file_type[i], c("_control_var.RDS"))))
    tic_means <- (readRDS(paste0(file_type[i], c("_tic_mean.RDS"))))
    tic_mean_mats <- (readRDS(paste0(file_type[i], c("_tic_mean_mat.RDS"))))
    tic_sum_mats <- (readRDS(paste0(file_type[i], c("_tic_sum_mat.RDS"))))

  } else {
    tic_sums <- rbind(tic_sums, ((readRDS(paste0(file_type[i], c("_tic_sum.RDS"))))))
```

```
  t100_vars <- rbind(t100_vars, (readRDS(paste0(file_type[i], c("_t100_var.RDS")))))
  t200_vars <- rbind(t200_vars, (readRDS(paste0(file_type[i], c("_t200_var.RDS")))))
  t300_vars <- rbind(t300_vars, (readRDS(paste0(file_type[i], c("_t300_var.RDS")))))
  control_vars <- rbind(control_vars, readRDS(paste0(file_type[i], c("_control_var.RDS"))))
  tic_means <- rbind(tic_means, readRDS(paste0(file_type[i], c("_tic_mean.RDS"))))
  tic_mean_mats <- rbind(tic_mean_mats, readRDS(paste0(file_type[i], c("_tic_mean_mat.RDS"))))
  tic_sum_mats <- rbind(tic_sum_mats, readRDS(paste0(file_type[i], c("_tic_sum_mat.RDS"))))
 }

}

## Total Intensity Change Plots for Different Capillaries, relative to each ambient tic
jpeg(file=paste0(c("C:/Users/asus/Documents/DESI_Data/All_iMZML/Plots/Total_Intensity_Change_All_Types")
             , exp_type, c(".png")))
y_max <- max(c(tic_sums[1,1:4]/tic_sums[1,1], tic_sums[2,1:4]/tic_sums[2,1],
           tic_sums[3,1:4]/tic_sums[3,1], tic_sums[4,1:4]/tic_sums[4,1],
           tic_sums[5,1:4]/tic_sums[5,1]))

plot(tic_sums[1,1:4]/tic_sums[1,1], type="o", col = "blue",
    main = paste0(c("Increase in Intensity Due to Temperature for Capillary Cross Sections")),
    xlab = "Experiment Temperature", ylab = "Factor Increase", ylim = c(1, y_max), xaxt = "n",
    cex.main=2, cex.lab=1.5, cex.axis=1.5, lwd = 3)
axis(1, at = 1:4, labels = temp_arr, cex.axis = 1.5)
lines(tic_sums[2,1:4]/tic_sums[2,1], type = "o", col = "red", lwd = 3)
lines(tic_sums[3,1:4]/tic_sums[3,1], type = "o", col = "black", lwd = 3)
lines(tic_sums[4,1:4]/tic_sums[4,1], type = "o", col = "green", lwd = 3)
lines(tic_sums[5,1:4]/tic_sums[5,1], type = "o", col = "orange", lwd = 3)
legend("topleft", legend=(exp_type), fill = c("blue", "red", "black", "green", "orange"),
      cex = 1.5 )
dev.off()

## Total Intensity Log10 Plots for Different Capillaries
jpeg(file=paste0(c("C:/Users/asus/Documents/DESI_Data/All_iMZML/Plots/Log_Intensity_All_Types"),
              exp_type, c(".png")))
plot(log10(tic_sums[1,1:4]), type="o", col = "blue",
    main = paste0(c("Temperature vs. log10(Intensity) for Capillary Cross Sections")),
    xlab = "Experiment Temperature", ylab = "log10(Total Intensity)", xaxt = "n",
    ylim = c(6, 10), cex.main=2, cex.lab=1.5, cex.axis=1.5, lwd = 3)
axis(1, at = 1:4, labels = temp_arr, cex.axis = 1.5)
lines(log10(tic_sums[2,1:4]), type = "o", col = "red", lwd = 3)
lines(log10(tic_sums[3,1:4]), type = "o", col = "black", lwd = 3)
lines(log10(tic_sums[4,1:4]), type = "o", col = "green", lwd = 3)
lines(log10(tic_sums[5,1:4]), type = "o", col = "orange", lwd = 3)
legend("topleft", legend=(exp_type), fill = c("blue", "red", "black", "green", "orange"),
      cex = 1.5)
dev.off()

## Total Intensity Plots for Different Capillaries
jpeg(file=paste0(c("C:/Users/asus/Documents/DESI_Data/All_iMZML/Plots/Total_Intensity_All_Types"),
               exp_type, c(".png")))
y_min <- min(c(tic_sums[1,1:4], tic_sums[2,1:4],
            tic_sums[3,1:4], tic_sums[4,1:4],
            tic_sums[5,1:4]))
y_max <- max(c(tic_sums[1,1:4], tic_sums[2,1:4],
            tic_sums[3,1:4], tic_sums[4,1:4],
            tic_sums[5,1:4]))

plot(tic_sums[1,1:4], type="o", col = "blue",
    main = paste0(c("Temperature vs. Intensity for Capillary Cross Sections")),
    xlab = "Experiment Temperature", ylab = "Total Intensity", xaxt = "n",
    cex.main=2, cex.lab=1.5, cex.axis=1.5, lwd = 3, ylim = c(y_min, y_max))
axis(1, at = 1:4, labels = temp_arr, cex.axis = 1.5)
lines(tic_sums[2,1:4], type = "o", col = "red", lwd = 3)
lines(tic_sums[3,1:4], type = "o", col = "black", lwd = 3)
lines(tic_sums[4,1:4], type = "o", col = "green", lwd = 3)
lines(tic_sums[5,1:4], type = "o", col = "orange", lwd = 3)
legend("topleft", legend=(exp_type), fill = c("blue", "red", "black", "green", "orange"),
      cex = 1.5)
dev.off()
```

```
## Sample-to-Sample Variation
boxplot(control_vars[1,],control_vars[2,], control_vars[3,], control_vars[4,],
      control_vars[5,], main = "Total Intensity at Ambient Temperature",
      outline = FALSE, xaxt = "n", lwd = 2,  ylab = "Total Intensity",
      xlab = "Capillary ID", cex.main=2, cex.lab=1.5, cex.axis=1.5,
      col = "#D98719")
axis(1, at = 1:5, labels = exp_type, cex.axis = 1.5)


## Stack matrices in a list and export to CSV
tic_sum_list <- list() ##Initialize tic sum list
for(i in  1:length(exp_type)){
  tic_sum_list[[i]] <- matrix(tic_sum_mats[i,],nrow = 4, ncol = 3, byrow = TRUE)
}

## Convert to data.frame and export to .csv
lapply(tic_sum_list, function(x) write.table( data.frame(x), append= T, sep=',',
                                    row.names = temp_arr,
                                    col.names = rep_arr,
                                    "TIC_SUMS.csv"))

tic_mean_list <- list() ##Initialize tic mean list
for(i in  1:length(exp_type)){
  tic_mean_list[[i]] <- matrix(tic_mean_mats[i,],nrow = 4, ncol = 3, byrow = TRUE)
}

## Convert to data.frame and export to .csv
lapply(tic_mean_list, function(x) write.table( data.frame(x), sep=',',
                                     row.names = temp_arr,
                                     col.names = rep_arr,
                                     "TIC_MEANS.csv"))

## Create Data Frames for Easy Viewing
tic_sums_df <- data.frame(tic_sums)
row.names(tic_sums_df) <- (exp_type)
names(tic_sums_df) <- (temp_arr)

tic_means_df <- data.frame(tic_means)
row.names(tic_means_df) <- (exp_type)
names(tic_means_df) <- (temp_arr
```

REFERENCES

[1] C. C. Hsu, “Effects of Heat Transfer on Ion Transfer Efficiency with Multichannel Capillaries,” Massachusetts Institute of Technology, 2020.

[2] B. J. Murphy, “The History of Jim Waters and Waters Corporation.” Oct-2015 [Online]. Available: https://www.waters.com/webassets/other/corp/about/assets/files/HistoryW.pdf. [Accessed: 22-Aug-2020]

[3] “About Waters : Waters.” [Online]. Available: https://www.waters.com/waters/en_US/About-Waters/nav.htm?locale=en_US&cid=134614448. [Accessed: 22-Aug-2020]

[4] “2019 Annual Report,” Waters Corporation [Online]. Available: https://waterscorporation.gcs-web.com/static-files/7178d06c-f04c-43fe-a598-074e3cdf1da6. [Accessed: 29-Aug-2020]

[5] “World Renown Service and Support : Waters.” [Online]. Available: https://www.waters.com/waters/en_US/World-Renown-Service-and-Support/nav.htm?locale=en_US&cid=505846. [Accessed: 29-Aug-2020]

[6] R. Batra, “Operational Analysis of an Inventory Location Optimization Algorithm and RFID Implementation in a Distribution Center,” Massachusetts Institute of Technology, 2018.

[7] D. Hochsztein, “Development and Implementation of an Inventory Location Optimization Algorithm for Improved Distribution Center Picking Rates,” Massachusetts Institute of Technology, 2018.

[8] S. Liu, “Design and Development of an Automated Inspection System for Vials,” Massachusetts Institute of Technology, 2019.

[9] B. Zeng, “Improved Packing Strategy for Distribution Centers to Reduce Freight Cost,” Massachusetts Institute of Technology, 2019.

[10] R. Lee, “Development of Solutions to Reduce Uneveness in Material Flow at a Factory,” Massachusetts Institute of Technology, 2020.

[11] Y. Wang, “Optimization of Material Flow by Lean Tools and RFID Integration into a Vendor-Involved eKanban System,” Massachusetts Institute of Technology, 2020.

[12] S. Borman, “MS History,” 26-May-1998. [Online]. Available: https://masspec.scripps.edu/mshistory/perspectives/sborman.php#link6. [Accessed: 30-Aug-2020]

[13] J. Clark, “The Mass Spectrometer,” *chemguide,* 2000. [Online]. Available: https://www.chemguide.co.uk/analysis/masspec/howitworks.html. [Accessed: 30-Aug-2020]

[14] C. Proteomics, “MALDI-TOF Mass Spectrometry,” *Creative Proteomics*. [Online]. Available: https://www.creative-proteomics.com/technology/maldi-tof-mass-spectrometry.htm. [Accessed: 05-Sep-2020]

[15] J. Fenn, M. Mann, C. Meng, S. Wong, and C. Whitehouse, “Electrospray ionization for mass spectrometry of large biomolecules,” *Science*, vol. 246, no. 4926, pp. 64–71, Oct. 1989, doi: 10.1126/science.2675315.

[16] Z. Takáts, J. M. Wiseman, and R. G. Cooks, “Ambient mass spectrometry using desorption electrospray ionization (DESI): instrumentation, mechanisms and applications in forensics, chemistry, and biology,” *J. Mass Spectrom.*, vol. 40, no. 10, pp. 1261–1275, 2005, doi: 10.1002/jms.922.

[17] “Quadrupole,” *An Introduction to Mass Spectrometry*. [Online]. Available: https://science.widener.edu/svb/massspec/intro_to_ms/quad.html. [Accessed: 05-Sep-2020]

[18] “QuanTof - High-resolution, accurate mass, quantitative time-of-flight MS technology,” Waters Corporation, 2013 [Online]. Available: https://www.waters.com/waters/library.htm?cid=511436&lid=134717600&lset=1&locale=en_US&changedCountry=Y. [Accessed: 05-Sep-2020]

[19] “SYNAPT G2-Si HDMS,” *Waters TA Materials Website*. [Online]. Available: https://materials.waters.com/synapt-g2-si-hdms/. [Accessed: 05-Sep-2020]

[20] L. Bernier, M. Taesch, S. Rauschenbach, and J. Reiss, “Transfer conditions and transmission bias in capillaries of vacuum interfaces,” *Int. J. Mass Spectrom.*, vol. 447, p. 116239, Jan. 2020, doi: 10.1016/j.ijms.2019.116239.

[21] W. Leveille, “DESI Heater Design Review,” Waters Corporation, 04-Nov-2019.

[22] B. Lin and J. Sunner, “Ion transport by viscous gas flow through capillaries,” *J. Am. Soc. Mass Spectrom.*, vol. 5, no. 10, pp. 873–885, Oct. 1994, doi: 10.1021/jasms.8b00489.

[23] S. Meyyappan, “Thermal Modelling.” 13-Jul-2020.

[24] E. R. Wouters, A. A. Makarov, R. P. ATHERTON, and J. J. Dunyach, “Ion Transfer Tube Having Single or Multiple Elongate Bore Segments and Mass Spectrometer System,” US20120043460A123-Feb-2012 [Online]. Available: https://patents.google.com/patent/US20120043460A1/en. [Accessed: 30-Aug-2020]

[25] “AISI Type 304 Stainless Stee,” *ASM Aerospace Specification Metals Inc.* [Online]. Available: http://asm.matweb.com/search/SpecificMaterial.asp?bassnum=MQ304A. [Accessed: 06-Sep-2020]

[26] “Special Metals INCONEL® Alloy 600,” *ASM Aerospace Specification Metals Inc.* [Online]. Available: http://asm.matweb.com/search/SpecificMaterial.asp?bassnum=NINC30. [Accessed: 06-Sep-2020]

[27] "Cartridge Brass, UNS C26000 (260 Brass), H00 Temper wire." [Online]. Available: http://www.matweb.com/search/DataSheet.aspx?MatGUID=2bca2e6b94244f47a6faece6e5cdb86f. [Accessed: 06-Sep-2020]

[28] "AISI Type 316 Stainless Steel, annealed sheet," *ASM Aerospace Specification Metals Inc.* [Online]. Available: http://asm.matweb.com/search/SpecificMaterial.asp?bassnum=MQ316A. [Accessed: 06-Sep-2020]

[29] "Vacuum Compatible Metals and Alloys," *Meyer Tool & Mfg.* [Online]. Available: https://www.mtm-inc.com/ac-20120328-vacuum-compatible-metals-and-alloys.html. [Accessed: 07-Sep-2020]

[30] A. Römpp *et al.*, "imzML: Imaging Mass Spectrometry Markup Language: A Common Data Format for Mass Spectrometry Imaging," in *Data Mining in Proteomics: From Standards to Applications*, M. Hamacher, M. Eisenacher, and C. Stephan, Eds. Totowa, NJ: Humana Press, 2011, pp. 205–224 [Online]. Available: https://doi.org/10.1007/978-1-60761-987-1_12. [Accessed: 09-Sep-2020]

[31] "Cardinal 2: User guide for mass spectrometry imaging analysis." [Online]. Available: https://www.bioconductor.org/packages/release/bioc/vignettes/Cardinal/inst/doc/Cardinal-2-guide.html#reading-continuous-imzml. [Accessed: 26-Aug-2020]